Jast
Vol. 16, No 2, June, 2025

JOURNAL

of

APPLIED SCIENCE

&

TECHNOLOGY

ISSN 2006-6775

Available Electronically!

w.w.w auchipoly.edu.ng

TABLE OF CONTENT

JOURNAL OF APPLIED SCIENCE AND TECHNOLOGY, VOL, 16, NO 2, JUNE, 2025. pp 1-12

ISSN: 2006- 6775

Fast Neutron Activation Analysis and Computation of Silica-Sand for High Strength Aluminosilicate (AI_2O_3-SiO_2) Glass Systems

[1,*] Iliya Ezekiel and [2]Amaakaven Victor Dhave

[1]*Department of Ceramic Technology, School of Applied Sciences & Technology, Auchi Polytechnic, Auchi.*

[2]*Department of Ceramic Technology, School of Sciences & Industrial Technology, Akanu Ibiam Polytechnic, Ebonyi*

[*]**Correspondence:** E-mail: eiliya@auchipoly.edu.ng

Abstract

Fast Neutron Activation Analysis (FNAA) and thermochemical computation using FactSage provide complementary approaches for the characterization and optimization of silica sand in the development of high strength aluminosilicate (Al_2O_3–SiO_2) glass systems. By integrating FNAA data into FactSage simulations, researchers can evaluate phase stability, identify potential crystallization pathways, and optimize thermal processing conditions. The synergy between experimental analysis and computational modeling supports the design of aluminosilicate glasses with enhanced mechanical strength, chemical durability, and thermal resistance. Such materials are vital for applications in aerospace, optics, and high-performance construction. This combined methodology underscores the importance of coupling nuclear analytical techniques with advanced thermodynamic computation to achieve reliable, scalable, and innovative glass formulations. Ultimately, FNAA and FactSage together provide a robust framework for advancing aluminosilicate glass technology. In this research, ceramic raw materials sample containing high amount of alumina (Al_2O_3) concentration of 18.88 wt.% and suitable concentration of silica (Si) of 46.76 wt.% for aluminosilicate glass system application are investigated by means of FNAA analysis and FactSage. The method evidence concentrations compatible with some commercial aluminosilicate glass systems formulas from measured data exploited from the nuclear data reactions of the experiment.

Keyword: Aluminosilicate glass, FNAA, Alumina, Silica, FactSage, Computation

Introduction

Aluminosilicate glasses typically (not always) contain boron oxide but are deemed aluminosilicate if they contain more alumina than boron oxide, on a molar basis (Kessler, Hornung, Keppler, Schorcht, Hellwing, Liebetrau, Körner, .Sävert, Siebold, Schnepp, Hein and Kaluza, 2014). Generally, they are the most refractory (high-temperature) of glasses containing alkali and alkaline earth modifiers. They have a relatively steep viscosity-temperature curve giving high and strain points, but are still meltable in conventional furnaces. A typical composition ranges from lower silica eutectics to calcium based eutectics. Aluminosilicate glass system have found important commercial applications as infrared transmitting glasses at 4um-5um wavelength, space shuttle window inner panes, tungsten-halogen lamp ampoule in automobile head lamps and for liquid crystal display (Zhang and Chen, 2025).

They are also abundant in nature and relevant for geological processes as they are chemically close to the natural magmatic compositions of the Earth mantle. Finally at low SiO_2 content, quenched metallurgical slags are mainly composed of aluminosilicate glasses. Introducing Al_2O_3 strongly affects many physico-chemical properties (Wani and Katiyar, 2025). For instance, it improves fracture strength, increases elastic modulus and chemical resistance or hinders the trend to phase separation. Many properties correlate with the nature of non-framework cations present in the glass and to the flexibility for Al to adopt multiple coordination states. Different aspects of the disorder (network connectivity, Si/Al disorder, short range environment) affect the topological and configurational entropies (Elsevier. (2025).

Aluminosilicate (AS) glasses, notably at low-alkali content, have high values of tensile strength, resistance to high temperature and excellence resistance to chemical corrosion (Varshneya and Mauro, 2019). They have found widespread commercial application as fibers to reinforce plastics or concrete. E-glass (a low-alkali Ca-Mg alumino-borosilicate glass with 10-15 mol.% Al_2O_3) is the most common glass fibers. Nowadays, a major application concerns alkali-free aluminosilicates used as thin glass sheets for liquid crystal flat displays. With higher amounts of alkalis, aluminosilicate glasses can be used to obtain high surface strength via an ion exchange process. The chemical exchange (typically Na replaced by K) produces a permanent compressive stress in the glass surface that improves resistance to cracks and scratches. This type of glass is exploited in smartphone screens or aircraft windshields and further applications (for instance in automotive) are foreseen. Alkali or alkaline-earth aluminosilicate systems are also the precursor glasses for most glass-ceramics successfully designed for consumer applications (Kumar and Singh, 2025).

Archetypically, the intermediate oxide nature of Al_2O_3 means that it is incapable of acting as a glass former because it does not satisfy the rules proposed by Zachariasen for a network former. However, a specificity of Al_2O_3 is to be able to form a glass when it is mixed 2 with some modifying cations (typically alkaline earths or rare-earths). Al_2O_3 is classified as an intermediate oxide acting as network former or modifier according to the composition. Indeed, Al_2O_3 can be added into the vitreous silicate network by replacing Si^{4+} cations in a tetrahedral environment. In that case, it plays the role of a network former and even small amounts of Al_2O_3 considerably modify the glass properties. Alternatively, Al can enter into high coordinated sites, playing the role of a modifier (Gupta and Sharma, 2025).

Si is a network former occurring as SiO_4 tetrahedra in oxide glasses. In aluminosilicate glasses, Al has a strong preference for tetrahedral coordination and usually substitutes for Si in tetrahedral positions, behaving similarly to a network former. An $Al^{3+}O4$ tetrahedron has a charge deficit compared to a $Si^{4+}O4$ unit because only three positive charges are brought by Al^{3+} cations. The electrical balance and the stabilization of (AlO_4)- tetrahedra are ensured by introducing positive charges brought by alkali (M^{+}), alkaline earth (M^{2+}) or rare-earth (RE^{3+}) cations. The cations compensating the net negative charge on (AlO_4)- units are called charge compensators (or charge balancing cations), as opposed to a network modifying role when they are associated with non-bridging oxygen atoms (NBOs), participating in this latter case to the loss of network connectivity (depolymerization). The introduction of Al_2O_3 results in less NBOs

(and thus more bridging oxygen atoms, BOs) and increases network connectivity. As a consequence the network becomes stiffer, the viscosity and the glass transition temperature (Tg) increase .

Since the Al-O bond length (1.76 Å) is longer than for Si-O (1.62 Å) (Cormier, Neuville, Calas, 2000), the AlO_4 tetrahedron is bigger than SiO_4. The replacement of Si by Al then modifies the network organization and changes the glass physico-chemical properties. Raman spectroscopic investigations of aluminosilicate glasses revealed that increasing the Al/Si ratio implies a decrease in the force constant due to the weakening of the T-O bonds (T = Si or Al) when Al substitutes for Si. The structure of aluminosilicate glasses largely depends on the arrangement of SiO_4 and AlO_4 tetrahedra that are forming a skeletal network by corner-sharing through bridging oxygen (BO) atoms (Cormier, 2021).

Since its first introduction in the late 1950s fast neutron activation analysis (FNAA) using the H(d,n) fusion reaction has become a well-established technique for bulk sample elemental analyses. It has been applied to detection of light elements such as carbon, nitrogen, oxygen, phosphorus, or chlorine to detect illicit materials, explosives or drugs, in biological and geophysical research and in online process control in the coal and cement industry. An important application represents the determination of the stoichiometry of new compounds in materials science. Nowadays, small compact deuterium-tritium neutron generators represent an accessible fast neutron source. Novel approach using FNAA shows that it can be deployed in determining the bulk elemental composition of Heusler alloys containing Mn, Fe, Al, Si, Sn using 14 MeV fast neutrons. It is applied to small samples of typical masses around 4 g because these new alloys are usually prepared in small amounts, but it can be scaled up to measure much larger samples with similar or even higher precision(Constantinescu, Bugoi, Constantin, Macovei, Dima, Garlea & Garlea, 1999).

The concentration of aluminosilicate in a silica sand sample for suitable application in alumina silicate glass systems are investigated by means of Fast Neutron Activation Analysis (FNAA)

Experimental

Fast Neutron Activation Analysis (FNAA) with 14 MeV neutron was used for determination of Al and Si concentration in the sample. The 14 MeV neutron generator is a KAMAN's model-711 sealed type. Accurate determination at Al and Si in the sand sample using neutrons depends on the choice of appropriate experimental conditions to avoid nuclear interference because of the juxtaposition of the two elements on the periodic table. Consequently, a procedure for the simultaneous determination of Al and Si contents of sand sample was developed based on an irradiation time and a counting time each of 5min using the low-yield of 14 MeV neutrons currently available in combination with a Nal (TI) detector.

Powdered sample of the sample mixed with organic liquid binder and pressed into pellets of 23mm diameter by a hydraulic press machine. High purity Al foil monitor fixed to the sample were take manually for irradiation at 15mm from the target cooling cap of the 14 MeV seal-tube neutron generator. The primary fast neutron flux reaching the samples was monitored by Al flux monitor fastened to the sample and

standards. Integral counts of a BF_3 neutron counter kept close to the target of the neutron generator were used to check variation of the flux. The present average neutron flux emitted by the neutron generator at an accelerating voltage of 13.0 kv and a bean current of 3. 8 mA measured try ^{27} Al (n,a)^{24} Na reaction was found to be 10^6 ncm $^{-2}5^{-1}$. Consequently, the irradiation and measuring times were appropriately chosen to be 300s to reduce the effects of the both spectral and nuclear interference on measured activities of the times of interest.

The γ-ray Spectrometer consists of a 760 x 760mm Nal (IT) scintillation detector, which has resolution of 0.07 at 662 keV line at ^{137} Cs. It is coupled to a computer multichannel analyser card sys2tem (PCAII).

Photos peak efficiency of the γ-ray spectrometer has been determined by dis-shaped standard γ-ray sources at near and far geometries in the 120-1860 keV energy region. For the analysis of Si, the 1779 keV line was used whereas for the analysis of Al, only the 843 keV line was considered because of the counting statistics of the 1014 keV line as a result of its low branching ratios. Nuclear data acceptable for this work is shown in Table1

.

Table 1: Nuclear data of reactions used in the experiment

Nuclear Reaction	Half Life	Cross Section(mb)	Gamma Energy(keV)	Gramma Integrity
^{27}Al(n,p)^{27} Mg	9.46min	75.0	843.70	72.0
			1014.4	28.0
^{27}Al(n,γ)^{28} Al	2.24min	05	1779.0	100.0
^{28}Si(n,p)^{28} Al	2.24min	226.0	1779.0	100.0
^{56}Fe(n,p)^{56}Mn	2.58h	103.0	846.8	98.9
			1810.7	27.2

In Table 2, comparable archaeometrical studies reveal first the possibility to determine light elements (O, Na, Mg, AI, and Si) was for the first time presented in. Within the frame of our archaeometrical program for Byzantine objects (coins, glasses, ceramics) we used FNAA as a complementary method to XRF (X-Ray Fluorescence) and PIXE (Particle Induced X-ray Emission). FNAA is a non-de-structive bulk analytical tool and the objective is to determine some light elements (Na, Mg, A1, Si, K), to solve the problem of interference (X-rays) in the case of As-Pb and to explore its possibilities for other major, minor and trace elements. We irradiated some Cu and Pb coins, glass and ceramics samples placed at 5 cm behind the Be target for 100 minutes with a current beam intensity of 8-9 pA (Q = 50 mC, corresponding to 5 - 1012 n/cm^2). The radionuclides formated (Table 1) were measured in two stages: after 30 min cooling time to determine Si, A1, Mg, K and after 72 h cooling time (for the others radioisotopes). Ortec HPGe detector (1.9 keV resolutions at 1332.5 keV and 25% relative efficiency) was used, connected to an 8192 channel Spectrum 88 MCA.

Computaion Simulation Using FactSage

FactSage 6.4 was utilizing to calculate the viscosity of the glasses obtained from different compositions: 100 wt% slag (100s), 80s20c and 60s40c, ass detailed in Table1. The glasses database was used

because it is applicable over the entire temperature range, including temperature at and below the glass transition temperature. Additionally, thermodynamic calculations were performed using FactSage™ to predict the phases that would form during solidification, employing the FToxid database and selecting the liquid solution FToxid_SLAGA (Katte, 2020: Online Glass Engineering, 2021: Materials Science Insights. 2019).

Matrix Method in Glass Batch Calculation

FactSage was deployed in matrix inversion to compute exact raw material weights and simulation of equilibrium phases and viscosity for aluminosilicate systems. The matrix method is a linear algebra approach to batch calculation. It ensures that the chosen raw materials (batch) yield the desired oxide composition (glass) after melting.

The general formula is:

$$N_B = (B^T \cdot B)^{-1} \cdot B^T \cdot N_G$$

N_B: column matrix of batch molarities (raw materials), N_G: column matrix of target glass molarities (oxides), B: batching matrix (oxide contributions from each raw material), B^T: transpose of batching matrix ans $(B^T \cdot B)^{-1}$: inverse matrix for solving linear system

From molarities, FactSage converts to weight percentages using molar masses of oxides and raw materials (Kundu, 2019: Online Glass Engineering, 2021: Wikipedia contributors, 2025).

Results and Discussion

Nuclear interference effect due to $^{27}Al(n,\gamma)^{28}$ Al reaction in the analysis of Si via the $^{28}Si(n,p)^{28}$ Al has been found to be negligible because of the low cross section value of the former in the 14 MeV neutron energy region. Similarly, spectral interference in the measurement of the peak area of 843 and 1779 KeV line by the 846 and 1810 KeV lines respectively produced by the activation of iron present in the sample via the $^{56}Fe(n,p)^{56}Mn$ reaction was found to be less than 0.1%. This value was determined by counting the samples again, exactly 1 hour after irradiation to allow for the complete decay of ^{27}Mg and ^{28}Al residual radio-nuclides.

The measured data used for the calculation of the concentrations of Al and Si in the samples are based on the equation below:

$$C_a = \frac{A_a M_s A_{fs} M_{fa}}{A_s M_a A_{fa} M_{fs}} \times 100\%$$

where C_a is the concentration in wt. % of the element in the sample, A_a the γ-ray peak count of the element in the standard, A_{fa} the γ-ray peak count of Al flux monitor of standard, M_a the mass of standard, M_a the mass of sample, M_{fs} the most of flux monitor of standard and M_{fa} the mass of the flux monitor of sample

. **Table 3:** Contains the calculated concentration of Al and Si sample

Sample Raw material	**Al_2O_3 (wt. %)**	**SiO_2 (wt. %)**
Silica Sand	18.88	46.76

Basis for selection of alumina silicate glass system from experimental results is based on high amount of Al_2O_3 from sample and by using conversion factors; the stoichiometry volume fraction of each oxide in the system can be calculated from the batch compositions of established formulas (Simmingskold, 1997).

In Table 2, Constantinescu et al., established that samples were put at 3 - 5 cm in front of the detector. Because of the broad energy spectrum, nuclear reactions such as (n,γ), (n, 2n), (n, p), (n, a) are easily produced and their interferences must be considered. The threshold values for (n, 2n) nuclear reactions are of the order of 10 MeV and taking into account the fact that there are very few neutrons with so high energies, observed only the reaction on Ca, As, Ag, Sb. For the Cu coins detected radioisotopes of Fe, Ni, Cu, Zn, As, Ag, Sn, Sb, Pb; for the Pb coins: Fe, Cu, Zn, As, Ag, Cd, In, Sn, Sb, Pb (interference In-Sn, Cd-In); for ceramics: Mg, A1, Si, K, Ca, Ti, Fe, Zr, Ba, Ce (interference Mg-A1-Si, Y-Zr) and for glass: Na, Mg, A1, Si, K, Ca, Fe, Cu, Zn, As, Ba, Ce, Pb (interference Na-A1, A1-Si) (Constantinescu et al, 1999).

The precision of our results is of the order of 15 to 25% relatively. The detection limits in our conditions are in the range of 30 (Ni, As, Sb) to 200 mg/kg (Ti, Fe, Zn, Sn, Ba, and Pb) for trace elements and in the range of 0.2 to 1% for major light elements. To calibrate the method, standards with an elemental composition close to glass and ceramics (e.g. major components SiO_2, Fe_2O_3, $A1_2O_3$, CaO, MgO, K_2O, and Na2O). The data in Table 2, provides with precision elementals such as silicon (Si^{4+}) and Aluminium (Al^{3+}) with nuclear data of reactions that are consistent with FNAA studies. For instance, both silicon (Si^{4+}: ($^{29}Si(n,p)$) and Aluminium (Al^{3+}: ($^{27}Al(n,p)$) are in good agreement with the nuclear reaction thresholds and half-life.

Table 2: Observed radioisotopes from established experiment (Constantinescu et al, 1999)

Element	Nuclear Reactor	Threshold (MeV)	Nuclide used	Half-life	Eγ(keV)
Mg	$^{24}Mg(n,p)$	4.93	^{24}Na	28.7h	1368.6
A1	$^{27}Al(n,p)$	1.9	^{27}Mg	9.45 min	1014
Si	$^{29}Si(n,p)$	3	$^{29}A1$	14.97h	1273
K	$^{41}K(n,p)$	1.75	^{41}Ar	6.5 min	1293.6
Ca	$^{43}Ca(n,p)$	1.06	^{43}K	1.83h	373
	$^{46}Ca(n,\gamma)$		^{47}Ca	22.3 h	271
Ti	$^{46}Ti(n,p)$	1.62	^{46}Sc	2.44d	889.3
	$^{48}Ti(n,p)$	3.27	^{48}Sc	83.8d	983.5
Fe	$^{54}Fe(n,\alpha)$	-	^{51}Cr	43.7h	320.5
	$^{54}Fe(n,p)$		^{54}Mn	27.7d	834.5
Ni	$^{58}Ni(n,p)$	-	^{58}Co	312.2d	810.8
Cu	$^{63}Cu(n,\alpha)$	-	^{60}Co	70.91d	1332.5
Zn	$^{67}Zn(n,p)$	-	^{67}Cu	5.272y	184.6
As	$^{75}As(n,2n)$	10.38	^{74}As	61.9h	595.9
Zr	$^{90}Zr(n,2n)$	12.07	^{89}Zr	17.78d	909.2
Ag	$^{107}Ag(n,2n)$	9.48	^{106}Ag	78.4h	451; 717
Cd	$^{114}Cd(n,\gamma)$	-	^{115}Cd	8.4d	336; 527
In	$^{113}In(n,\gamma)$	-	^{114m}ln	2.224d	189.9
Sn	$^{117}Sn(n,n')$	-	^{117m}Sn	49.5d	158.5
	$^{116}Sn(n,\gamma)$	-	^{117m}Sn	14d	158.5

Sb	^{121}Sb(n,2n)	9.36	^{120m}Sb	14d	197; 1023
	^{121}Sb(n,γ)		^{122}Sb	5.76d	564
Ba	^{135}Ba(n,n')	-	^{135m}Ba	2.72d	268.2
	^{134}Ba(n,γ)	-	^{135m}Ba	28.7h	268.2
Pb	2^{04}Pb(n,2n)	6.97	^{203}Pb	51.88h	279

3.1 Computer-Aided Batch Calculation

Computer-aided batch calculation applied for computation of high-strength glass using silica sand with 18.88 wt.% Al_2O_3 and 46.76 wt.% SiO_2 is as follows:

Step 1: Define target glass composition

For a high-strength aluminosilicate glass, a typical target might be:

- SiO_2 = 65 wt.%
- Al_2O_3 = 12 wt.%
- CaO = 10 wt.%
- MgO = 8 wt.%
- Na_2O = 5 wt.%

Table 4: Building contribution matrix of each raw material contributes oxides (FactSage™)

Raw Material	SiO_2	Al_2O_3	Na_2O	CaO	MgO
Silica sand	0.4676	0.1888	0	0	0
Alumina	0	1.00	0	0	0
Soda ash	0	0	0.585	0	0
Dolomite	0	0	0	0.560	0
Dolomite	0	0	0	0	0.44

Step 2: Input raw material data

The computer-aided batch calculation software requires the oxide composition of each raw material. For example:

- Silica sand: 46.76% SiO_2, 18.88% Al_2O_3, balance inert.
- Pure silica (SiO_2): 100% SiO_2.
- Alumina (Al_2O_3): 100% Al_2O_3.
- Dolomite ($CaMg(CO_3)_2$): yields 0.56 CaO + 0.44 MgO.
- Soda ash (Na_2CO_3): yields 0.58 Na_2O.

Step 3: Build the matrix

The software sets up a system of linear equations:

$[A.x = b]$

Where:

- (A) = oxide contribution matrix from raw materials
- (x) = unknown batch weights of raw materials
- (b) = target oxide composition vector

$$\begin{bmatrix} 0.0466 & 1.0 & 0 & 0 & 0 \\ 0.1888 & 0 & 1.0 & 0 & 0 \\ 0 & 0 & 0 & 0.56 & 0 \\ 0 & 0 & 0 & 0.44 & 0 \\ 0 & 0 & 0 & 0 & 0.58 \end{bmatrix} \begin{bmatrix} x_1 \\ x_2 \\ x_3 \\ x_4 \\ x_5 \end{bmatrix} = \begin{bmatrix} 0.65 \\ 0.12 \\ 0.10 \\ 0.08 \\ 0.05 \end{bmatrix}$$

Step 4: Solve (Computer-Aided Gaussian Elimination)

The software applies matrix inversion or Gaussian elimination:

- From CaO: $x_4 = 0.10 / 0.56 = 0.179$
- From MgO: $x_4 = 0.08 / 0.44 = 0.182$ (consistent)
- From Na_2O: $x_5 = 0.05 / 0.58 = 0.086$
- From SiO_2: $0.4676x_1 + x_2 = 0.65$
- From Al_2O_3: $0.1888x_1 + x_3 = 0.12$

Table 5: Raw materials and parts

`Raw Material	**Parts (wt.%)**
Silica sand	34.1
Pure silica	39.4
Alumina	3.8
Dolomite	15.3
Soda ash	7.3

Final Computer-Aided Batch Composition

This recipe yields a high-strength aluminosilicate glass with ~65% SiO_2, 12% Al_2O_3, and balanced modifiers (CaO, MgO, Na_2O).

Computer-Aided Batch (CAB) calculation without additional pure silica

Employing CAB matrix process for your silica sand composition (18.88 wt.% Al_2O_3 and 46.76 wt.% SiO_2) under the condition that no additional pure silica is added.

Step 1: Define the Problem

Choosing $x_1 = 0.40$:

- $x_2 = 0.463$
- $x_3 = 0.045$

So solution vector:
x = [0.40, 0.463, 0.045, 0.18, 0.086]

Step 5: Normalize to 100 Parts

Total = 1.174 → Normalize:

- Raw material: Silica sand (contains both SiO_2 and Al_2O_3).
- Constraint: No extra pure silica can be added.
- Goal: Formulate a glass batch with high alumina strength by balancing oxides using other raw materials (e.g., alumina, soda ash, limestone).

Step 2: Normalize Oxide Composition

From silica sand:

- Al_2O_3 = 18.88 wt.%
- SiO_2 = 46.76 wt.%

- Balance ≈ 34.36 wt.% (other oxides, ignored for now).

This is already alumina-rich, but not yet balanced for glass formation.

Normalized (SiO_2 + Al_2O_3 only):

- SiO_2 = 71.24%
- Al_2O_3 = 28.76%

Step 3: Target Glass Composition

For high-strength alumina glass, literature-based target (Shelby, 2005):

- SiO_2 ≈ 65–70%
- Al_2O_3 ≈ 20–25%
- Na_2O ≈ 5%
- CaO ≈ 5%

Target vector (*b*):

$$b = \begin{bmatrix} 0.67 \\ 0.23 \\ 0.05 \\ 0.05 \end{bmatrix}$$

Step 4: Contribution Matrix (No Pure Silica)

Since no pure silica is allowed, silica sand must supply all SiO_2. Other raw materials supply Al_2O_3, Na_2O, and CaO

Table 6: Raw materials and matrix precursor of aluminosilicate (FactSage™)

Raw Material	**SiO_2**	**Al_2O_3**	**Na_2O**	**CaO**
Silica sand	0.4676	0.1888	0	0
Alumina	0	1.00	0	0
Soda ash	0	0	0.585	0
Limestone	0	0	0	0.560

Matrix (*A)*:

$$A = \begin{bmatrix} 0.4676 & 0 & 0 & 0 \\ 0.1888 & 1 & 0 & 0 \\ 0 & 0 & 0.585 & 0 \\ 0 & 0 & 0 & 0.56 \end{bmatrix}$$

Equation:

[$A.\ x = b$]

Where:

- (x) = batch weights of raw materials
- (b) = target oxide composition

Step 5: Solve the Matrix Equation

Using MATLAB/Python (linear algebra solver):

```
A = [0.4676 0     0     0;
     0.1888 1.0   0     0;
     0      0   0.585   0;
     0      0     0   0.560];

b = [0.67; 0.23; 0.05; 0.05];

x = A\b;
x_normalized = x / sum(x);
batch_weights = x_normalized * 1000; % grams for 1 kg batch
```

Step 6: Example Batch Result (Approximate)

For 1 kg batch:

- Silica sand ≈ 650 g
- Alumina ≈ 230 g
- Soda ash ≈ 70 g
- Limestone ≈ 50 g

This yields ~67% SiO_2, 23% Al_2O_3, 5% Na_2O, 5% CaO — a high-strength alumina glass composition, achieved without adding pure silica.

Step 7: Validation (Computer-Aided)

- Run equilibrium in FactSage/ThermoCalc at 1500–1600 °C.
- Confirm liquid phase stability (avoid mullite crystallization).
- Use viscosity module to check melt processability.
- Adjust fluxes if viscosity is too high.

The table below 4; shoes some commercial aluminosillicate glass system formulas

Table 4: Harper's† basis for some aluminosilicate glass systems

Oxides	**SiO_2**	**Al_2O_3**	**CaO**	
(Wt. %)	31.7	29.0	27.1	Lower silica eutectics
	58.0	20.0	16.0	Calcium base eutectice
	62.1	14.60	23.3	
	57.0	24.20	6.80 †	

Conclusions

Fast Neutron Activation Analysis (FNAA) combined with computational batch design in FactSage provides a powerful framework for optimizing silica-sand based aluminosilicate glass systems. FNAA offers high sensitivity for detecting trace elements in raw materials, ensuring that silica sand and alumina sources meet stringent purity requirements. This analytical precision is critical for high-strength aluminosilicate glasses, where even minor impurities can alter viscosity, durability, and mechanical performance. By quantifying elemental composition with FNAA, researchers can input accurate oxide data into FactSage's matrix method, which systematically balances raw material inputs against desired oxide outputs. The matrix approach transforms batch calculation into a solvable linear algebra problem, allowing precise determination of silica sand, alumina hydrate, and flux requirements. FactSage's AD module further refines this process by accounting for decomposition reactions, loss on ignition, and equilibrium phase stability. Together, FNAA and computational modeling ensure reproducibility, cost efficiency, and performance optimization in industrial glass production. FNAA indicates high alumina concentration and appropriate silica concentration of the sample from nuclear data reaction and calculated measurement. The aluminosilicate concentration is within the purview of some selected commercial batch formulas for both lower silica eutectics and calcium based eutectics. Ultimately, this integration bridges experimental analysis with digital computation, enabling the design of aluminosilicate glasses with tailored properties for high-strength applications. It highlights the synergy between advanced nuclear analytical techniques and thermochemical software, paving the way for sustainable and scientifically rigorous glass manufacturing.

Reference

- Constantinescu, B., Bugoi, R., Constantin, F., Macovei, M., Dima, S., Garlea, C., & Garlea, I. (1999). Fast neutron activation analysis—FNAA using d(13 MeV) + Be reaction for archaeometrical research at Bucharest cyclotron. *Czech Journal of Physics, 49*(Suppl 1), 385–388. https://doi.org/10.1007/s10582-999-0050-3

- Cormier, L. (2021). Glasses: Aluminosilicates.In *Encyclopedia of materials: Technical ceramics and glasses* (pp. 496–518). Elsevier.https://doi.org/10.1016/B978-0-12-818542-1.00076-X (doi.org in Bing)

- Doyle, P. J. (1998). *Glass making today*. Portcullis Press.

- Elsevier. (2025). *Advanced ceramic materials* (Elsevier Series in Advanced Ceramic Materials). Elsevier.

- Griteo, A., Moldovan, R., & Simon, V. (2005). Thermal and infrared analyses of aluminosilicate glass

hysterias for dental implants. *Journal of Optoelectronics and Advanced Materials, 7*(6), 2847–2852.

- Gupta, A., & Sharma, N. (2025). *Design and microstructure control in advanced ceramics*. CRC Press.
- Harper, C. (2001). *Handbook of ceramics, glasses, and diamonds*. McGraw-Hill.
- Katte, H. (2020). The economic significance of batch calculation in glass production. Ilis GmbH. https://www.ilis.de
- Kessler, A., Hornung, M., Keppler, S., Schorcht, F., Hellwing, L., Liebetrau, H., Körner, J., Sävert, A., Siebold, M., Schnepp, M., Hein, J., & Kaluza, M. (2014). 16.6 J chirped femtosecond laser pulses from a diode-pumped Yb:CaF_2 amplifier. *Optics Letters, 39*(5), 1333–1336. https://doi.org/10.1364/OL.39.001333 (doi.org in Bing)
- Kumar, R., & Singh, P. (2025). *Emerging technologies in advanced ceramics: Processing and performance*. Springer.
- Kundu, R. (2019). *Glass batch calculations – Chapter 2 experimental*.Maharshi DayanandUniversity. Retrieved from Studocu.
- Materials Science Insights. (2019). Glass batch formulation: Materials and considerations. https://materialsscience.com
- Online Glass Engineering. (2021). Batch compositions and formula management for glassproducers.https://glassengineering.com
- Pelton, A. D., Degterov, S. A., & Eriksson, G. (2000). The FactSage thermochemical software and databases. *Calphad, 24*(2), 189–228. https://doi.org/10.1016/S0364-5916(00)00029-0
- Shelby, J. E. (2005). *Introduction to glass science and technology* (2nd ed.). Royal Society of Chemistry.
- Simmingskold, B. O. (1997). *Raw materials for glass melting*. Elsevier.
- Wani, M. F., & Katiyar, J. K. (2025). *Advancedceramics: Innovations in tribology and high-temperature applications*. BookAuthority.
- Wikipedia contributors. (2025). Glass batch calculation. In *Wikipedia*.Retrieved February 13, 2026, from https://en.wikipedia.org/wiki/Glass_batch_calculation
- Zhang, Y., & Chen, L. (2025). *Functional ceramics for energy and environment*. Wiley.

JOURNAL OF APPLIED SCIENCE AND TECHNOLOGY, VOL, 16, NO 2, JUNE, 2025. pp 13- 20

ISSN: 2006- 6775

COMPARATIVE EFFECT OF SOLVENT POLARITY ON THE ANTIMICROBIAL PROPERTIES OF SOME INDIGENOUS PLANT SPECIES.

[1]Dibua Redeemed Ihmimoya, [2]Ohagim Joy, [3]Ajikobi Rapheal Ayodeji, [4]Aperua-Yusuf Kalimat Iyamah, [5]Joshua Oyanna Salami[e]

[1,3,4] Department of Biochemistry, School of Applied Science and Technology, Auchi Polytechnic Auchi.

[b]Department of Science laboratory Technology, School of Applied Science and Technology, Auchi Polytechnic Auchi.

[5]Department of Microbiology, School of Applied Science and Technology, Auchi Polytechnic Auchi.

Corresponding author: redeemed.dibua@gmail.com

ABSTRACT

This study investigated the comparative effect of solvent polarity on the antimicrobial properties of selected indigenous plant species, namely *Ocimum gratissimum* (scent leaf), *Telfairia occidentalis* (ugwu leaf), plantain flour, and yam flour. Different solvents of varying polarities—n-hexane (non-polar), ethyl acetate (moderately polar), ethanol, and methanol (polar)—were used to extract bioactive compounds from the samples using cold method extraction. The antimicrobial activities of the extracts were evaluated against two microorganisms; *Pseudomonas aeruginosa* and *Bacillus subtilis*, using the agar well diffusion method, while minimum inhibitory concentrations (MIC) were determined via broth dilution. Results revealed that solvent polarity significantly influenced the antimicrobial efficacy of the extracts. Polar bioactive compounds exhibited higher antimicrobial activity in leafy samples, while non-polar solvents showed selective effectiveness 7.50mm (*Telfairia gratissium*), 8mm (*ociumum gratissimum),* for *Pseudomonas* while they had 14mm for *Bacillus*. *Ocimum gratissimum* and *Telfairia occidentalis* demonstrated stronger antimicrobial properties compared to plantain and yam flours. Notably, *Bacillus subtilis* (14mm) wasmore susceptible to most extracts than *Pseudomonas aeruginosa* (7.50mm and 8mm). The findings highlight the importance of solvent selection in optimizing the extraction of bioactive compounds and support the potential use of these indigenous plants as natural antimicrobial agents.

Keys words: solvent polarity, antimicrobial activity, bioactive compounds, extraction methods, *ociumum gratissimum, Telfaira occidentails.*

INTRODUCTION

Medicinal plants have long been harnessed for their therapeutic properties, largely due to their robust phytochemical consistent, including phenolics, flavonoids, and other antioxidant compounds. In Nigeria, *Ocimum gratissimum* (locally known as scent leaf) and *Telfairia occidentalis* (locally known as fluted pumpkin or ugwu) are widely consumed leafy vegetables well-known for their nutritional and medicinal benefits. These plants are essential to traditional diets and are held to own various health-promoting properties, including antioxidant

activities that fight oxidative stress-related diseases (Akinmoladun *et al.,* 2022).

Also, Plantain and yam are major staples foods in many parts of Africa, including Nigeria. Beyond their nutritional value, these crops are rich in phytochemicals with potential antimicrobial properties, which can be harnessed for food preservation and medicinal purposes (Chanda *et al.,* 2020). Recent studies have underscored the significance of extraction methods and solvent polarity in influencing the efficiency of bioactive compound isolation from plant materials (Sowbhagya, 2020).

Solvent polarity refers to the ability of a solvent to dissolve polar substances. Polar solvents, such as methanol and ethanol, are effective in extracting polar compounds like phenolics and flavonoids, which are known for their antioxidant properties. Conversely, non-polar solvents, such as hexane, are more suitable for extracting non-polar compounds like lipids. The choice of a suitable solvent or solvent combination is crucial for efficient extraction of desired phytochemicals (Akinmoladun *et al.,* 2022). Solvent polarity plays a critical role in determining the types and quantities of phytochemicals extracted, thus affecting the antimicrobial activity of the extracts (Zhang *et al.,* 2021).

The extraction of bioactive compounds from plant materials is a critical step in evaluating their antioxidant potential. Solvent extraction is the most commonly employed method, and the choice of solvent significantly influences the yield and efficacy of the extracted compounds. Solvent polarity, in particular, plays a pivotal role in determining the solubility of phytochemicals, thereby affecting both the quantity and quality of the extracts obtained (Wakeel *et al.,* 2019). Recent studies have highlighted the influence of solvent polarity on the extraction yield and antioxidant capacity of various plant materials. For instance, Wakeel *et al.* (2019) investigated the effect of solvent polarity on the phytochemical yield and antioxidant capacity of Isatis tinctoria and found that solvent polarity significantly affects total phenolic content (TPC) and total flavonoid content (TFC), with higher yields observed in solvents with intermediate polarity.

Antimicrobial properties refers to the ability of a plant to inhibit the growth of microorganism. Studies have revealed that sent leaf has a broad-spetum antimicrobial properties this could be attributed to the presence of the essential; oil found in the plant. Also, ugwu leaf have equally shows promising antimicrobial activity due to its rich phytochemicals content. (Wakeel *et al.,* 2019). The antioxidant and antimicrobial properties of *Ocimum gratissimum* and *Telfairia occidentalis* have been documented in various studies. For example, Akinmoladun *et al.* (2022) demonstrated that extracts of Chrysophyllum albidum exhibited significant antioxidant activities, which were influenced by the extraction solvent and method used. These findings underscore the potential of these plants as sources of natural antioxidants and the importance of optimizing extraction conditions to harness their full therapeutic potential.

Despite the recognized health benefits of *Ocimum gratissimum* and *Telfairia occidentalis*, there is a paucity of studies examining the effect of solvent polarity on the antimicrobial properties of these specific plants. Most existing research has focused on other plant species, leaving a gap in the literature regarding the optimal extraction conditions for maximizing the antioxidant potential of scent leaf and ugwu leaf. Addressing this gap is crucial for developing standardized extraction protocols that can be employed in the production of nutraceuticals and functional foods derived from these

plants (Wakeel *et al.*, 2019; Akinmoladun *et al.*, 2022).

Despite growing interest in natural antimicrobials, limited research has been conducted on the influence of solvent polarity on the antimicrobial potential of processed food flours, particularly plantain and yam, from Auchi metropolis (Ogunbanwo *et al.*, 2022). This study aims to fill this gap by evaluating how different solvent polarities affect the antimicrobial properties of different indigenous plants, thereby contributing to safer food preservation strategies and enhancing the value of these local crops

MATERIALS AND METHODS

Materials

Chemicals and reagents

Nutrient agar, ethyl acetate, n-hexane, methanol, sterile water.

Equipment

Hot air oven, autoclave, inoculation loop, petri dish, digital weighing balance, cork borer, blender.

Sample Collection

Fresh samples of plantain (*Musa* Paradisiaca), yam (*Dioscorea* roundata), uguw leave (*Telfauria occidnetalis*) and sent leave (*Ocimum gratissimum*) were procured from major local markets within Auchi metropolis, Etsako West Local Government Area. Edo State, Nigeria. Samples were authenticated by a botanist, (Humphery Ukponaye Eguasa), in the department of Science Laboratory Technology, Auchi Polytechnic. Voucher specimens were prepared, pressed, and deposited Auchi Polytechnic Herbarium for reference. The following voucher numbers were assigned:

i. *Musa paradisiaca* (Plantain) AP/VH/2024/001
ii. *Dioscorea rotundata* (yam) AP/VH/2024/002
iii. *Telfairia occidentalis* (Ugwu) AP/VH/2024/003
iv. *Ocimum gratissium* (sent leave) AP/VH/2024/004

Preparation of samples

The plants samples were thoroughly washed with clean water to remove dirt. They were peeled, sliced into uniform thin pieces (for the tubers), and dried using a hot-air oven at 50°C until constant weight was achieved (approximately 48–72 hours). The samples were milled into fine flour using a mechanical grinder and sieved through a 250 µm mesh. The flours were stored in airtight containers at room temperature until extraction.

Solvent Extraction

Solvents of varying polarities were used

- Non-polar solvent: n-hexane

- Moderately polar solvent: ethyl acetate

- Polar solvent: methanol and distilled water.

20 g of each homogenised was weighed into a separate conical flask. 200 mL of solvent was added (solid-to-solvent ratio 1:10 w/v). The mixture was agitated on a mechanical

shaker at 120 rpm for 48 hours at room temperature (25–28°C). Extracts were filtered through Whatman No. 1 filter paper. Solvents were evaporated under reduced pressure using a rotary evaporator at appropriate temperatures. Aqueous extracts were freeze-dried (Agrawal *et al.,* 2024).

Test Microorganisms

Standard strains of bacteria and fungi were obtained from Auchi polytechnic Auchi microbiology laboratory collection. Selected organisms included:

- Gram-positive bacteria: *Staphylococcus aureus, Bacillus subtilis*

- Gram-negative bacteria: *Escherichia coli, Pseudomonas aeruginosa*

- Fungi: *Candida albicans, Aspergillus niger*

Test organisms were maintained on nutrient agar (bacteria) sub-cultured before use (Chatepa *et al.,* 2024).

Preparation of Inoculum

A loopful of each microorganism was transferred into 10 mL sterile normal saline. Turbidity was adjusted to match 0.5 McFarland standard (approximately 1.5 × 10^8 CFU/mL).

Antimicrobial Activity Assay

The antimicrobial activities of the extracts were evaluated using the agar well diffusion method (Dai *et al.,* 2020).

Procedure:

Mueller-Hinton Agar (MHA) plates (for bacteria) was prepared. Plates were seeded with 0.1 mL of standardized inoculum using sterile swabs. Wells (6 mm diameter) were bored into the agar with a sterile cork borer. Each well was filled with 100 µL of extract solution at concentrations of 100 mg/mL. Plates were allowed to stand for 1 hour for diffusion at room temperature before incubation (Dibacto *et al.,* 2024).

- Incubation:

- Bacterial plates: 24 hours at 37°C

- Fungal plates: 48–72 hours at 28°C

Controls:

- Positive controls: Standard antibiotics (e.g.,ciprofloxacin for bacteria, ketoconazole for fungi)

- Negative control: Solvent used for extraction without the sample

Measurement:

Zones of inhibition (clear areas around wells) were measured in millimeters (mm) using a transparent ruler. Each test was performed in triplicates and the mean inhibition zone was recorded (Dibacto *et al.,* 2024; Mehmood *et al.,* 2022).

Minimum Inhibitory Concentration (MIC) Determination

MIC of active extracts was determined by the broth dilution method.

Serial two-fold dilutions of extracts (ranging from 100 to 6.25 mg/mL) were prepared. Each dilution was inoculated with 100 µL of standardized microbial suspension. Tubes were incubated under appropriate conditions. MIC was recorded as the lowest concentration showing no visible growth (Gonçalves *et al.,* 2020).

RESULT

Table 1 Effect of solvent polarity on the antimicrobial properties of ugwu leaf

S/N	Solvents	Isolate	Agar well	Agar diffusion
1.	N- hexane	Pseudomonas	7.50mm	Nil
		Bacillus	23.00mm	22.00mm
2.	Ethylaceate	Pseudomonas	12.00mm	Nil
		Bacillus	14.00mm	Nil
3.	Ethanol	Pseudomonas	13.00mm	8.60mm
		Bacillus	27.50mm	6.00mm
4.	Methanol	Pseudomonas	10.50mm	2.00mm
		Bacillus	24.00mm	2.40mm

Table 2 Effect of solvent polarity on the antimicrobial properties of sent leaf

S/N	Solvents	Isolate	Agar well	Agar diffusion
1.	N- hexane	Pseudomonas	Nil	Nil
		Bacillus	38mm	25mm
2.	Ethylaceate	Pseudomonas	8mm	9mm
		Bacillus	14mm	7mm
3.	Ethanol	Pseudomonas	Nil	Nil
		Bacillus	37mm	15mm
4.	Methanol	Pseudomonas	12mm	9mm
		Bacillus	20.5mm	Nil

Table 4.3 Effect of solvent polarity on the antimicrobial properties of plantain flour

S/N	Solvents	Isolate	Agar well	Agar diffusion
5.	N- hexane	Pseudomonas	10.05mm	7.00mm
		Bacillus	9.00mm	Nil
6.	Ethylaceate	Pseudomonas	Nil	7.50mm
		Bacillus	Nil	Nil
7.	Ethanol	Pseudomonas	6.50mm	6.50mm
		Bacillus	Nil	Nil
8.	Methanol	Pseudomonas	5.00mm	Nil
		Bacillus	Nil	Nil

Table 3 Effect of solvent polarity on the antimicrobial properties of Yam flour

S/N	Solvents	Isolate	Agar well	Agar diffusion
1.	N- hexane	Pseudomonas	Nil	Nil
		Bacillus	Nil	Nil
2.	Ethylaceate	Pseudomonas	Nil	9mm
		Bacillus	Nil	Nil
3.	Ethanol	Pseudomonas	Nil	9mm
		Bacillus	Nil	Nil
4.	Methanol	Pseudomonas	Nil	8mm
		Bacillus	Nil	Nil

DISCUSSION

The findings of this study clearly demonstrate that solvent polarity plays a critical role in determining the antimicrobial effectiveness of plant extracts. The variation observed across different solvents can be attributed to their differential ability to dissolve specific phytochemicals. Polar solvents such as methanol and ethanol are particularly effective in extracting phenolic compounds, flavonoids, and other polar bioactive constituents. As noted by Sowbhagya (2020), polar solvents are more efficient in extracting phenolic and flavonoid compounds due to their high solubility in such media. These compounds are widely associated with antimicrobial activity because they can disrupt microbial membranes and interfere with metabolic processes (Wakeel *et al.*, 2019). This explains the relatively higher inhibition zones observed in ethanol and methanol extracts, particularly in *Ocimum gratissimum* and *Telfairia occidentalis.*

In contrast, n-hexane, a non-polar solvent, showed limited antimicrobial activity in most cases, although it demonstrated notable effectiveness against Bacillus subtilis in scent leaf extracts. This suggests that non-polar solvents extract lipophilic bioactive compounds such as essential oils and terpenoids. According to Chanda *et al.* (2020), plant-derived antimicrobial agents include essential oils and terpenoids which exhibit activity primarily against specific microorganisms. This supports the selective antimicrobial activity observed with n-hexane extracts. Ethyl acetate, being moderately polar, exhibited intermediate effects, which aligns with the findings of Zhang *et al.* (2021), who reported that solvent polarity significantly influences both the yield and composition of extracted antioxidant compounds.

The results also revealed that leafy vegetables (*Ocimum gratissimum* and *Telfairia occidentalis*) exhibited significantly higher antimicrobial activity compared to plantain and yam flours. This can be attributed to their richer phytochemical composition. Akinmoladun *et al.* (2022) emphasized that the antioxidant and bioactive properties of plant materials are strongly dependent on their phytochemical composition and extraction method. Leafy plants are known to contain higher concentrations of phenolics, alkaloids, and essential oils, which contribute to their strong antimicrobial properties. Conversely, the relatively low antimicrobial activity observed in plantain and yam flour extracts may be linked to processing effects. Ogunbanwo *et al.* (2022) noted that processing methods can influence the antimicrobial activity of plant-derived food products by altering phytochemical availability.

Furthermore, *Bacillus subtilis* was generally more susceptible to the plant extracts than *Pseudomonas aeruginosa.* This difference in susceptibility can be explained by variations in cell wall structure. Gram-positive bacteria such as Bacillus subtilis lack the outer membrane present in Gram-negative bacteria. As highlighted by Chanda et al. (2020), Gram-negative bacteria possess an outer membrane that limits the penetration of many antimicrobial agents. This structural barrier likely contributed to the reduced susceptibility of Pseudomonas aeruginosa observed in this study.

Overall, the findings of this study are consistent with previous research emphasizing the role of solvent polarity in extraction efficiency and antimicrobial potential. Wakeel *et al.* (2019) reported that "solvent polarity mediates phytochemical yield and biological activity," while Zhang *et al.* (2021) further confirmed that solvent selection is crucial for optimizing bioactive compound recovery. These observations

reinforce the importance of selecting appropriate solvents to maximize the therapeutic and preservative potential of plant-derived compounds.

In summary, the observed variations in antimicrobial activity across different solvents and plant samples highlight solvent polarity as a key determinant in phytochemical extraction and biological efficacy. The integration of these findings with existing literature strengthens the reliability of the study and underscores the need for optimized extraction strategies.

CONCLUSION

This study confirms that solvent polarity has a significant impact on the antimicrobial properties of plant extracts. Polar solvents, particularly ethanol and methanol, were more effective in extracting bioactive compounds with strong antimicrobial activity, especially from *Ocimum gratissimum* and *Telfairia occidentalis*. Non-polar solvents showed selective activity, indicating the presence of different classes of bioactive compounds. Among the samples studied, leafy plants demonstrated superior antimicrobial potential compared to plantain and yam flours. Additionally, *Bacillus subtilis* was more susceptible to the extracts than *Pseudomonas aeruginosa*, highlighting differences in microbial resistancepatterns**.**

RECOMMENDATION

The need for careful selection of extraction solvents in phytochemical and antimicrobial studies. Further studies are recommended to isolate and characterize the specific bioactive compounds responsible for the observed activities and to explore their mechanisms of action.

REFERENCES

Agrawal, A., Sharma, P., and Singh, R. (2024). Plant antimicrobials: Extraction, characterization, and activity against foodborne microorganisms. *Folia Microbiologica*. Advance online publication.

Akinmoladun, F.O., Falaiye, O. E., Ojo, O. B., Adeoti, A., Amoo, Z. A., and Olaleye, M. T. (2022). Effect of extraction technique, solvent polarity, and plant matrix on the antioxidant properties of *Chrysophyllum albidum G. Don* (African Star Apple). *Bulletin of the National Research Centre*, 46(1), 40.

Chanda, W., Joseph, T. P., Tiash, S., and Mandal, R. K. (2020). Plant-derived antimicrobial compounds and their potential applications against bacterial infections. *Microbial Pathogenesis*, 150, 104675.

Chatepa, L. E. C., Mwamatope, B., Chikowe, I., and Masamba, K. G. (2024). Effects of solvent extraction on phytoconstituents and in vitro antioxidant activity of selected medicinal plants. *BMC Complementary Medicine and Therapies, 24*, 317.

Dai, Y., van Spronsen, J., Witkamp, G. J., Verpoorte, R., and Choi, Y. H. (2020). Natural deep eutectic solvents as new potential media for green technology: Enhanced antimicrobial activity of plant extracts. *BMC Chemistry, 14*(1), 1–12.

Dibacto, G., Alemayehu, M., and Tesfaye, B. (2024). Ethnomedicinal uses, antibacterial activity, and phytochemical screening of selected

medicinal plants. *BMC Complementary Medicine and Therapies*. Advance online publication.

Gonçalves, S., Gomes, D., Costa, P., Romano, A., and Rodrigues, A. E. (2020). Comparison of extraction techniques and solvents on antimicrobial and antioxidant potential of plant extracts. *Antibiotics, 9*(2), 48.

Mehmood, A., Shah, A., Khan, F., and Ali, S. (2022). Comparative analysis of solvent extraction methods for bioactive compounds and antimicrobial activity in medicinal plants. *Journal of Applied Biology and Biotechnology*, *10*(3), 45–53.

Ogunbanwo, S. T., Olalekan, B. K., and Olabode, O. A. (2022). Antimicrobial activity of some Nigerian food plants and influence of extraction solvents. *Journal of Medicinal Plants Research, 16*(3), 56–64.

Sowbhagya, H. B. (2020). Extraction of bioactive compounds: An overview of solvent extraction and implications. *Critical Reviews in Food Science and Nutrition, 60*(10), 1761–1776.

Wakeel, A., Jan, S. A., Ullah, I., Shinwari, Z. K., and Xu, M. (2019). Solvent polarity mediates phytochemical yield and antioxidant capacity of *Isatis tinctoria*. *PeerJ, 7*, e7857.

Zhang, M., Duan, C., Zhai, X., Li, S., and Ma, Y. (2021). Effect of solvent polarity on extraction of antioxidant compounds from plant materials. *Food Science and Technology*, 41(1), 147–155.

JOURNAL OF APPLIED SCIENCE AND TECHNOLOGY, VOL, 16, NO 2, JUNE, 2025. pp 21- 34

ISSN: 2006- 6775

Harnessing Wearable Technologies for Climate Change Resilience: A Multidisciplinary Approach to Biological and Economic Adaptation

Ukpoireghe Ibidayo Aliu [1*], Misheck Musaigwa [2], Olugbemiga Ojo Aliu [3], Clinton Aigbavboa [4], Patience Tunji-Olayeni [5]

[1] Department of Construction Management & Quantity Surveying, Faculty of Engineering and the Built Environment, University of Johannesburg, Johannesburg, 2006, South Africa

[2] Department of Business Management, University of Johannesburg, Johannesburg, South Africa.

[3] Department of Environmental Biology, School of Applied Sciences and Technology,Auchi Polytechnic, Auchi. Nigeria.

[4,5] Cidb Centre of Excellence, Faculty of Engineering and the Built Environment, University of Johannesburg, Johannesburg 2006, South Africa

Corresponding author's E-mail: bldrdayoaliu@gmail.com

Abstract.

The escalating impacts of climate change necessitate innovative solutions to enhance resilience and mitigate risks to human health and well-being. Despite the growing body of knowledge available on Climate Change effects and technological advancements and solutions, the effects still occur regularly, bringing diseases and even death.The methodology used for this study is a mixed approach. This paper explores the potential of wearable technologies as adaptive tools for monitoring and addressing climate-related challenges by integrating climate science, biological sciences, and economics perspectives, to examine how wearable devices can track key physiological and environmental parameters, such as heat stress, hydration levels, and air quality exposure, to safeguard human health in a changing environment; examine interrelations between biodiversity ecosystems and Climate Change with Nature-based solutions (NbS). The research also evaluates the economic feasibility and market dynamics of deploying wearable technologies at scale, emphasizing cost-effective solutions for vulnerable populations. By bridging disciplines, this study highlights the synergistic potential of technology, biology, and economics to create a robust framework for resilience and adaptation. The results show that from 2022.6 to 2022.8 we have optimization 18/ 77 , systems 16/183 , climate change 11/41, barriers 9/58, industry 4.0 is 7/52, the COVID-19 pandemic 6/31. The findings underscore the need for policy innovation, public-private partnerships, and user-centered design to ensure the equitable and widespread adoption of wearable technologies and NbS in the fight against climate change.

Keywords: Harnessing Wearable Technologies · Climate Change · Resilience · Biological · Economic Adaptation

Introduction

Despite the growing body of knowledge on Climate Change effects which greatly influences ecosystems and biodiversity by altering temperatures, rapid extreme weather conditions, increasing CO_2, altering rainfall patterns, aggravating seawater rise, drought, heat waves, wildfires, storms, and floods (Finlayson & van Dam, 22023), together with technology advancement solutions, these effects still occur regularly bringing diseases and even death. Hence, this exploratory study, Harnessing Wearable Technologies for Climate Resilience: A multidisciplinary Approach to Biological and Economic Adaptation. The methodology used for this study is a mixed approach. Interdisciplinary collaboration promotes interactions between natural and human systems, fosters innovation, and helps create sustainable, inclusive strategies to tackle environmental problems on a global scale (Wu, 2025; Burroughs, 2001)

This study aims to explore the potential of wearable technologies as adaptive tools for monitoring and addressing climate-related challenges by tracking key physiological and environmental parameters to safeguard human health in a changing environment, by economic feasibility, as well as explore nature-based solutions (NbS) for managing biodiversity and ecosystem resilience against climate change. In light of this, the following objectives are to achieve this aim- i) to examine wearable technology devices for tracking heat stress, ii) to examine wearable technology devices for tracking hydration levels, iii) to examine wearable technology devices for tracking air quality exposure, to safeguard human health in a changing environment, iv) to examine interrelations between biological sciences and climate change , v) to examine-nature based solutions for climate and ecosystem resilience, vi) to evaluate the economic feasibility and market dynamics of deploying wearable technologies at scale, for vulnerable populations. vii) to examine Wearable Technologies cost-effective solutions for vulnerable populations, viii) to determine the frequently researched keywords for the subject matter of the focus area.

Research Methodology

The research methodology employed qualitative and quantitative design. The review was based on previous literature of peer-reviewed journals from databases such as Google Scholar, Scopus, Web of Science, ResearchGate, and Academia, were used to access articles related to wearable technology for tracking heat stress, hydration, and air quality, biological science and climate change, and economic feasibility. In addition, a bibliometric review was conducted because of its robustness (Chadegani et al, 2013) to determine the most researched keyword and ascertain the area of focus for the subject matter for its justification. Bibliometric analysis can be described as the mathematical analysis of literature and their properties, such as authors, type of document, and timeline, as well as the visualization of the physical aspect of the scientific research in conjunction with the use of mapping tools of immersive (Babalola et al, 2023). A bibliometric analysis of articles is a beneficial analysis method as it shows the interactions among included articles, which clarifies how researchers have established an even distribution between quality, quantity, and the impact of such studies (Qiao et al, 2021). Furthermore,

bibliometric analysis contributes to effective research planning and multidisciplinary/interdisciplinary collaborations.

Document Retrieval

The selection criteria used to access articles related to wearable technology for tracking heat stress, hydration, and air quality**,** biological science, and climate change, and economic feasibility were by using the search keywords "wearable technologies and climate change**,**" research areas-all fields, the year 2020-2025 was set to retrieve the most recent articles. It retrieved 66 articles (46 articles, 20 Review Articles). In addition, the search keywords "biological science and climate change and nature-based solutions" were used to search through the databases mentioned above for related articles for the study. While the search keywords "wearable technologies and climate change and economic feasibility" were used for relevant materials for economic feasibility in the databases stated above.

In conducting the bibliometric review, the initial search keywords applied to verify the title, abstract, and keywords of the papers collected from the Web of Science database are Harnessing Wearable Technologies or Climate Change or Resilience, or Biological or Economic Adaptation, retrieved 411 articles. Further refinement was done to refine results for Harnessing Wearable Technologies or Climate Change or Resilience or Biological and Economic Adaptation (All Fields) and Engineering or Construction Building Technology (Research Areas) and English (Languages) and Business Economics (Research Areas) and Article (Document Types) and 2021 or 2022 or 2023 or 2024 or 2025 (Final Publication Year) and 2020 or 2021 or 2022 or 2023 or 2024 (Publication Years). These churned out 336 articles. Figure 3 shows the research framework for bibliometric analysis. The results presented in this study were derived from journal articles because they were subjected to peer review rather than books. The same applies to the most frequent research keywords and research focus of Harnessing Wearable Technologies for Climate Change Resilience: A Multidisciplinary Approach to Biological and Economic Adaptation, based on the year of publication

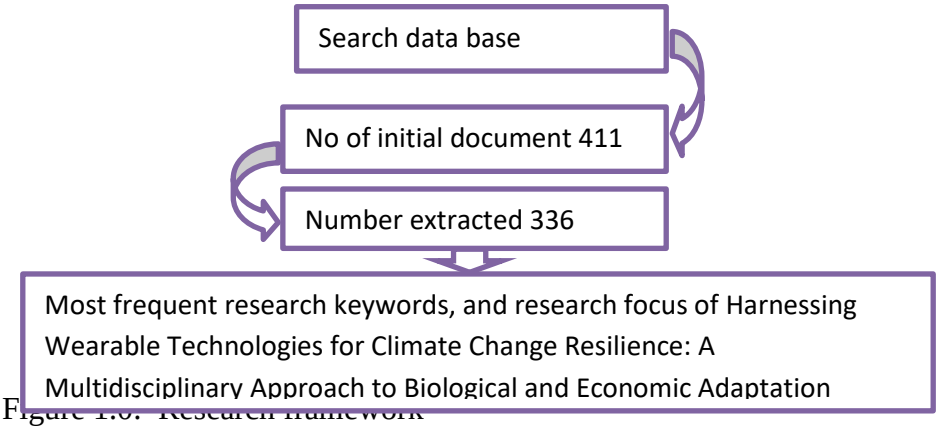

Figure 1.0: Research framework

Similarly, based on the bibliographic data collected, a co-occurrence map was produced to examine the co-occurrence of keywords extracted, which was done using the VOSviewer software, which can analyze large data, present the results in network

visualization maps and overlay visualization maps depicting the relations and strengths between the keywords, which are not frequently achieved with graphical illustrations.

Analysis, Results, and Discussions

Wearable technologies for monitoring heat stre**ss**-Intensively hot environment more than the average temperature can hinder the thermal homeostasis of the human body and bring about different sicknesses such as cardiovascular deaths, respiratory diseases, neurological disorders , infectious diseases, heat related damages, metabolic disorders, and mental disorders causing harm to human body wellness (Ganesan et al, 2018; Woychik et al, 2022; Pennisi, 2020; Wu et al, 2023; Ohtsuka et al, 2024; Gao et al, 2018). Sequel to this, wearable personal thermoregulation technologies are now available to manage heat stress (Wu et al, 2023). Though it has four types, such as Static thermoregulation which is easy to use ,sustainable, cost effective (Lei et al, 2023), but is limited by its inability to respond to changing environment; passive adaptive Thermoregulation is very effective for external environments (Li et al, 2021), energy economy, but limited by its inability to be controlled when neccessary; actively adaptive Thermoregulation automatically enables users to sustain customized thermal comfort even with different metabolic and environmental conditions (Chen et al, 2023) and the active cooling system which is based on external works to improve heat transfer for example, thermoelectric device (TED), (Hong et al, 2019) liquid cooling circulation, (Shvartz, 1975) and air ventilation, (Yi et al, 2017) can successfully provide much greater cooling power, can serve as first-aid equipment in extreme weather conditions and health-threatening situations that needs a strong cooling demand, but its non-energy economy.

Wearable technologies for monitoring hydration level : Wearable technologies have been designed to monitor body hydration for optimal function because the human body suffers from Dehydration due to much perspiring/sweating due to too much sunlight and heat due to changes in weather patterns (Gunda et al 2025). Some of the wearables are the AutoHydrate monitoring wearable, which automatically detects water drinking and physical activities (Mengistu et al, 2016), it is also very compact and handy and can be worn conveniently for more extended periods, uses real-time feedback; the IoT Hydration monitoring wearable technology is very economical (Singh et al, 2024); the Kenzen Wearable Device alert workers when they reach temperature thresholds that predispose workers to heat-related injuries and illnesses (Moyen et al, 2021); Nix Hydration Biosensor system, worn on the bicep to report estimated whole-body fluid loss and net electrolyte mass loss, enabling hydration-guidance features such as an Apple Watch alert upon the loss of 16 oz of sweat; Lastly is the Epicore hydration device which continuously streams sweat rate and electrolyte concentration i.e sodium and fluid loss (Davis et al, 2024).

Wearable technologies for monitoring air quality exposure when air is more polluted than ever because of climate change, it may result in diseases such as asthma, bronchitis, tuberculosis, and death (Khomenko et al, 2021). In light of these, wearable technologies and portable sensors have emerged to provide hope for acquiring air quality-related parameters, providing real-time data and monitoring (Dimitri et al, 2025), and creating awareness of pollution's and climate change's effects (Vitanza et al,

2023). Wearable technology enables people to plan their daily indoor or outdoor activities in areas that are minimally devoid of pollution so that areas prone to pollution can be treated or sanitized. These wearables include WeAIR, which uses geo-localization data and cloud-based platforms to conduct real-time air quality measurements, and it is compact and easily worn around (Dimitri et al, 2025); Atmo Wearable is a light and compact device used to track air quality in real-time by detecting and measuring pollutants such as PM2.5, PM10, CO2 and substances injurious to health like Volatile Organic Compounds (VOC) (Dimitri et al, 2025), and providing personalized information through a mobile app; Flow 2 device, developed by Plume Labs , measures similar pollutants like Atmo but, NO_2 (Nitrogen dioxide) in place of CO_2, while the information retrieved is shown on a mobile app to enable users have clarity to know and decide on the quality of the air in their environs.

Climate Change drivers and their impact onBiological Systems: Climate change(CC) drivers are greenhouse gas emissions, deforestation, agriculture, industrial activities, land use changes, volcanic eruptions, sun radiation, and ocean currents and cycles (Agathokleous et al, 2024), which stress the ecosystem, minimizing biodiversity, endangering the sustenance, equilibrium, and its essence. Their impact is as follows:

Temperature changes, Extreme Weather conditions, and loss of habitat.- Temperature changes around the globe/regions can alter species distribution, compelling migration to cooler or warmer areas, to prevent extinction and disruption of ecological balances. Extreme weather conditions such as heatwaves, tsunamis, droughts, and storms now occur very frequently and intensely due to CC, which destroys ecosystems and habitats, disrupts food and water sources, and narrows the survival of many species. Habitat Loss occurs due to rising temperatures and extreme weather, destroying habitats such as forests, human communities, wetlands, and coral reefs. Again, urbanization, deforestation, and agricultural practices lead to habitat loss, limit wildlife space, species food exploration, reproduction, migration routes, and cause fragmentation (Wudu et al, n.d.)

.

Nature-Based Solutions for Climate and Ecosystem Resilience (NBS for CER)

Reforestation and Afforestation Projects (RaAP)- Reforestation focuses on replanting trees in deforested areas, while afforestation involves planting trees in areas that were not initially forested (Turner et al, 2022). Furthermore, improved forest management (IFM) can be employed to counter greenhouse gas emissions (Griscom, 2017). Mitigating CC by sequestering carbon, enhancing biodiversity, preventing soil erosion, and improving water cycles, enables ecosystem resilience and sustainable land management (Wudu et al, n.d.).

Wetland Restoration for Carbon Capture- refers to the leading marine and coastal ecosystems for carbon capture and storage, such as mangroves, sea grass meadows, salt marshes, and kelp forests (Li, 2018). Mangroves and rainforests can sequester four times as much carbon dioxide per unit of area, Donato et al., (Wudu et al, n.d.) This improves biodiversity, water quality,

reduces floods, and ecosystem resilience (Hueholt et al, 2024).

Agroecological Practices Promoting Soil Health and Carbon Sequestration. Agroecological practices, such as crop rotation, agroforestry, and reduced tillage, promote soil health by enhancing biodiversity, improving soil structure, and increasing organic matter. These practices contribute to sequestering soil carbon, reducing greenhouse gas emissions, and improving resilience to climate impacts (Ahmad & Leung, 2023). In alignment with sustainable agriculture and ecosystem stability.

Economic feasibility and market dynamics of deploying wearable technologies for vulnerable populations: Barteit et al. (Barteit, 2021) examine the viability of employing consumer-grade wearables to assess the health consequences of climate change in resource-limited environments like Burkina Faso and Kenya. Their research demonstrates that the incorporation of wearable technology in these settings can enable communities by offering instruments to evaluate their environmental exposures and related health concerns (Barteit, 2021). Binyamin and Hoque (2020) examined the factors influencing the adoption of wearable health-monitoring devices, positing that accessibility and familiarity with these technologies are crucial for their acceptance (Binyamin & Hoque, 2020). Similarly, (Talukder et al, 2019), opined that the effective characteristics of wearable technology influence customer behavior and prospective market expansion. With the expansion of the wearable technology market, its incorporation into daily health management environments is anticipated to rise, especially in areas confronting environmental difficulties like CC. Multiple studies emphasize that wearable gadgets can improve health monitoring and furnish essential data that empower vulnerable people especially children (Saltzman & Hansel, 2024). (Nherera et al, 2021) highlight the significance of economic analysis in the use of wearable technologies for health interventions. Their research illustrates that including cost-effectiveness analysis in the use of wearable patient sensors might enhance patient outcomes while optimising healthcare resources (Nherera et al, 2021). Furthermore, recent research by Zaleski (2023) examines how wearable technologies can provide scalable health behavior interventions, thereby democratising access to health data across various socioeconomic strata and effectively fulfilling public health requirements. The persistent reduction in the price of wearable devices, llustrates a promising trend that enhanced affordability favors adoption among vulnerable populations.

Research Focus

In processing the most frequent research keywords, the benchmark of 5 was set to capture as much important data as possible for leveraging and providing chances for relevant areas that may be repressed since the data is big (336 articles) and the study is from 2000-2025. However, upon refinement, 128 keywords emerged as the most frequently researched out of 2,070 total keywords, and 5 cluster groups with 128 items (co-occurring words) were developed. See the network visualization of co-occurrent keywords in Figure 4.1below.

Findings

Findings shows that wearable personal thermoregulation technologies for tracking heat stress has four types. Some are easy to use, sustainable, cost effective (Lei et al, 2023) efficient for external environs (Li et

al, 2021) energy economy, sustains users customized thermal comfort amid varied metabolic and environmental conditions (Chen et al, 2023) provides more cooling power, can serve as first-aid equipment in extreme weather conditions and health-threatening situations that needs a strong cooling demand (Yi et al, 2017). However, some are limited by their inability- to respond to changing environment, to be controlled at will, and non-energy economy.

Findings reveal that wearables for tracking hydration include the AutoHydrate (Mengistu et al, 2016) which is very compact, handy and can be worn conveniently for more extended periods, uses real-time feedback; the IoT Hydration monitoring wearable technology is very economical (Singh et al, 2024) the Kenzen Wearable Device alert workers of risky temperature (Moyen et al, 2021); Nix Hydration Biosensor system, reports evaluated whole-body fluid loss and net electrolyte mass loss, while the Epicore hydration device continuously streams sweat rate and electrolyte concentration i.e sodium and fluid loss (Davis et al, 2024).

When air becomes more polluted because of climate change, it may result in diseases such as asthma, bronchitis, tuberculosis, and death (Khomenko et al, 2021). In light of these, wearable technologies and portable sensors have emerged to provide hope for acquiring air quality-related parameters, providing real-time data and monitoring (Dimitri et al, 2025), and creating awareness of pollution and climate change's effects (Vitanza et al, 2023). Wearable technology enables people to plan their daily indoor or outdoor activities in areas that are minimally devoid of pollution, so that areas prone to pollution can be treated or sanitized.

These wearables include WeAIR, which uses geo-localization data and cloud-based platforms to conductreal-time air quality measurements, and it is compact and easily worn around (Dimitri et al, 2025); Atmo Wearable is a light and compact device used to track air quality in real-time by detecting and measuring pollutants such as PM2.5, PM10, CO_2 and substances injurious to health like Volatile Organic Compounds (VOC) , and providing personalized information through a mobile app; Flow 2 device, developed by Plume Labs (Dimitri et al, 2025) measures similar pollutants like Atmo but, NO_2 (Nitrogen dioxide) in place of CO_2, while the information retrieved is shown on a mobile app to enable users have clarity to know and decide on the quality of the air in their environs.

Nature-Based Solutions for Climate and Ecosystem Resilience: among i**s** reforestation which focuses on replanting trees in deforested areas, while afforestation involves planting trees in areas that were not previously forested (Wu et al, 2025) Wetland Restoration for Carbon Capture which comprise of the marine and coastal ecosystems used for carbon capture and storage, such as mangroves, sea grass meadows, salt marshes, and kelp forests (Li, 2018). The mangrove and rainforest are very effective in sequestering carbon dioxide. Agroecological Practices can be employed in Promoting Soil Health and Carbon Sequestration through crop rotation, agroforestry, and reduced tillage, assist to promote soil health by enhancing biodiversity, improving soil structure, and increasing organic matter, which contribute to sequestering carbon, reducing greenhouse gas emissions, and improving resilience to climate impacts (Gao et al, 2018).

Cost-effective solutions identified for vulnerable populations: The investigation of wearable technologies as economical solutions for vulnerable populations,

especially in relation to concerns presented by climate change, including heat stress, air quality decline, and hydration problems, has received considerable focus in recent scholarly works. Nherera et al. (2021) highlight the significance of economic analysis in using wearable technologies for health interventions. Their research illustrates that including cost-effectiveness analysis in using wearable patient sensors might enhance patient outcomes while optimizing healthcare resources (Nherera et al., 2021). Considering the economic difficulties faced by these low-resource communities in Burkina Faso and Kenya; utilising affordable wearables gives a significant possibility to enable data-driven health interventions within budgetary limitations. The persistent reduction in the price of wearable devices, illustrates a promising trend that enhanced affordability favors adoption among vulnerable populations.

Findings from the bibliometric review shows the year time frame, frequently research keywords focus area, and the occurrences/total link strengths as follows: from 2022.6 to 2022.8 we have optimization 18/ 77 , systems 16/183 , climate change 11/41, barriers 9/58, industry 4.0 is 7/52, the COVID-19 pandemic 6/31, as shown in purple. See Figure 4.1 on the Overlay visualization map for frequently researched keywords for details. Then from 2022.8 (i.e., 2nd quarter) to 2023.0 focused on resilience 116/728, management 77/472, model 46/240, framework 39/242, supply chain resilience 34/200, sustainability 23/134 as depicted in dark green areas. Again, from 2023.0 to 2023.2 (1st quarter), the focus was on performance 74/460, innovation 34/226, organizational resilience 15/101, and risk-management 11/107, which are portrayed in light green. In addition, from 2023.2 to 2023.4, focused on Covid-19 38/285, disruptions 16/127, and integration 11/102, which is found in the lemon-green area. However, the research took a different turn from 2023.4 upwards as portrayed in yellow and in descending order of occurrences to focus on Impact 48/281, Dynamic capabilities 28/203, Organizations 22/172, Technology 20/112, Business 17/39, Disruptions 6/127, Supply chain 15/81,Pandemics 15/148, Collaboration 13/70, Big data 11/78, Transportation 11/76, Sustainable development 11/90, Firm performance 10/96, Big data analytics 9/72, Digital transformation 8/39, Decision making 7/52, Digitalization 7/59, Industry 4.0 7/48, Stress 7/42, Health 7/35, Transformation 7/42, Research and development 7/51, Crisis 6/46, Industry 6/35, Real-time systems 6/58, Manufacturing 6/59, Common method bias 5/45, Behavior 5/26, Ecosystems 5/32, Empirical-evidence 5/45, Critical infrastructure 5/24, Supply chain integration 5/35, Machine learning 5/14, IoT 5/24, Cost 5/41, and Security 5/39

.

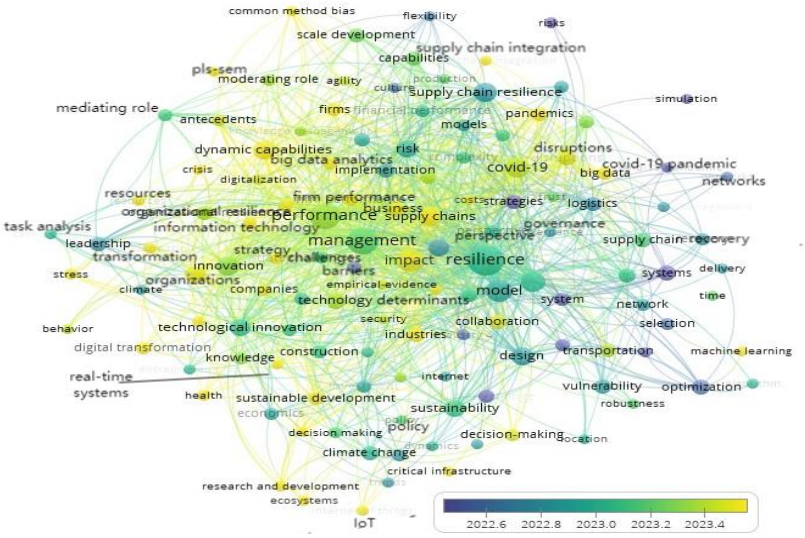

Figure 2.0: Overlay visualization map for most frequent research keywords

The research findings show that the focus area for 2023.2 to 2023.4, represented in lemon, is still under the category that requires more research because much impact has not been made; hence, it's in lemon green. Furthermore, findings show that the focus area for 2023.4 upwards is entirely dominated by yellow, which implies that much impact has not been attained at all; hence, it calls for research attention.

CONCLUSION

In Harnessing Wearable Technologies for Climate Change Resilience through a Multidisciplinary Approach to Biological and Economic Adaptation, the study revealed that the impact of CC on our environment is alarming, such as heat stress, hydration, polluted air leading to diseases and even deaths, disruption of biodiversity and ecosystems. In addition, the various solutions to tackle them economically are revealed, such as the adoption of wearable technology for tracking heat stress, hydration, and air quality, and NbS for managing the disruptions in our biodiversity and ecosystem. Wearable Thermoregulation efficiently tracks heat stress and can serve as first-aid equipment in extreme weather conditions and health-threatening situations that need a strong cooling demand, though not without limitations such as non-energy saving and inability to be controlled on demand. Furthermore, wearables for tracking hydration are numerous, can be worn conveniently for more extended periods, use real-time feedback, are very economical (Singh et al, 2024), alert workers of risky temperature (Moyen et al, 2021) and report evaluated whole-body fluid loss and net electrolyte mass loss (Davis et al, 2024). In tackling polluted air because of climate change, to avert diseases such as asthma, bronchitis, tuberculosis, and death (Khomenko et al, 2021), air tracking wearable technologies and portable sensors have emerged to provide hope for acquiring air quality-related parameters, providing real-time data and monitoring (Dimitri et al, 2025). Again, it creates awareness of pollution and climate change's effects (Vitanza et al, 2023). Wearable technology enables people to plan their daily indoor or outdoor activities in areas that are minimally devoid of pollution, so that areas prone to pollution can be treated or sanitized. Concerning the effects of CC drivers on biodiversity and the ecosystem, Nature-

Based Solutions for Climate and Ecosystem Resilience were suggested, such as reforestation and afforestation projects, wetland restoration for carbon capture, agroecological practices promoting soil health and carbon sequestration. Cost-effective solutions were identified for vulnerable populations, such as utilising affordable wearables, which gives a significant possibility to enable data-driven health interventions within budgetary limitations (Barteit et al., 2021). Furthermore, the persistent reduction in the price of wearable devices, illustrates a promising trend that enhanced affordability which favors adoption among vulnerable populations. After the bibliometric review, the most frequently investigated keywords emerged with clusters and co-occurring words. In addition the findings from the bibliometric review show that, by the second quarter of 2022, the research focused on resilience framework and models for covid 19 and pandemic management in disruptive environments as shown in the purple area; From 2022.6 (i.e., 2nd quarter) to 2022.8 (3rd quarter), the research focused on Technology impact on supply chain resilience amid risk and uncertainty as depicted in dark green areas; From 2022.8 (i.e., 3rd quarter) to 2023.0 to 2023.2 (1st quarter), research focused on Industrial Technological Innovation Sustainability in the face of Climate Change as shown in light green area; From 2023.2 to 2023.4 the focus was on Organizational innovative management performance and dynamic capabilities as portrayed in lemon green implying it is still under the category that requires more research because much impact has not been made; hence, it's in lemon green. Furthermore, findings show that the focus area for 2023.4 upwards is entirely dominated by yellow, which implies that much impact has not been attained at all; hence, it calls for research attention. As it focuses on the Impact of Dynamic capabilities of Organizational Technology on Business, Pandemics Disruptions, Supply chain, Collaboration, Big data, Transportation, Sustainable development and Firm performance. This study will contribute to knowledge in the following ways: the real-time monitoring/tracking by wearable for heat stress, hydration, air quality data will enable people to make decisions beneficial for their health and safety wellbeing against climate change; data retrieved from these wearables is going to assist government policies on public health and climate adaptation strategies; also assisting to identify trends and areas requiring intervention for example like the elderly, pregnant mothers and children. This aligns with the requirement for evidence-based approaches in addressing climate effects. Furthermore, the NbS for preserving the biodiversity and the ecosystem is going to assist policymakers in the planning and implementation strategies for natures preservation. Again, the interdisciplinary collaborations enables sharing different perspectives on how to tackle climate change technologically, naturally and economically. The limitation to this study stems from the use of Web of Science as the singular data base that was used for the bibliometric review to avoid any duplication. However, for future research other data bases may be included.

REFERENCES

Agathokleous, E., Feng, Z., Frei, M., Jiao, S., & Burkey, K. O. (2024). Response and adaptation of agricultural ecosystems to global changes. *Agriculture, Ecosystems & Environment*, *362*, 108844. https://doi.org/10.1016/j.agee.2023.108844

Ahmad, M., & Leung, C. C. (2023). Introduction: Climate change and environmental health. *The Yale Journal of Biology and Medicine*, *96*(2), 157.

Babalola, A., Manu, P., Cheung, C., Yunusa-Kaltungo, A., & Bartolo, P. (2023). A systematic review of the application of immersive technologies for safety and health management in the construction sector. *Journal of Safety Research*. https://doi.org/10.1016/j.jsr.2023.01.007

Barteit, S. (2021). Feasibility, acceptability and validation of wearable devices for climate change and health research in low-resource contexts of Burkina Faso and Kenya: Study protocol. PLOS ONE, 16(9), e0257170. https://doi.org/10.1371/journal.pone.0257170

Binyamin, S. S., & Hoque, M. R. (2020). Understanding the drivers of wearable health monitoring technology: An extension of the unified theory of acceptance and use of technology. *Sustainability, 12*(22), 9605.

Burroughs, W. J. (2001). Climate change: A multidisciplinary approach. Cambridge University Press.

Chadegani, A. A., Salehi, H., Yunus, M. M., Farhadi, H., Fooladi, M., Farhadi, M., & Ale Ebrahim, N. (2013). A comparison between two main academic literature collections: Web of Science and Scopus databases. arXiv. https://arxiv.org/abs/1305.0377

Chen, T.-H., Li, Z., Yang, P., Wang, H., Zhang, X., Liu, Y., & Fan, S. (2023). A kirigami-enabled electrochromic wearable variable-emittance device for energy-efficient adaptive personal thermoregulation. PNAS Nexus, 2(6), pgad165. https://doi.org/10.1093/pnasnexus/pgad165

Davis, N., Heikenfeld, J., Milla, C., & Javey, A. (2024). The challenges and promise of sweat sensing. *Nature Biotechnology*, *42*(6), 860–871. https://doi.org/10.1038/s41587-023-02059-1

Dimitri, G. M., Parri, L., Vitanza, E., Pozzebon, A., Fort, A., & Mocenni, C. (2025). WeAIR: Wearable swarm sensors for air quality monitoring to foster citizens' awareness of climate change. *Computer Standards & Interfaces*, *94*, 104004. https://doi.org/10.1016/j.csi.2025.104004

Finlayson, C. M., & van Dam, A. A. (2023). Climate change and wetlands: Vulnerability, adaptation, mitigation, resolutions, and scientific societies. In P. A. Gell, N. C. Davidson, & C. M. Finlayson (Eds.), Ramsar wetlands (pp. 495–524). Elsevier.

Ganesan, S., Summers, C. M., Pearce, S. C., Gabler, N. K., Valentine, R. J., Baumgard, L. H., & Rhoads, R. P. (2018). Short-term heat stress altered metabolism and insulin signaling in skeletal muscle. *Journal of Animal Science, 96*(1), 154–167.

Gao, W., Brooks, G. A., & Klonoff, D. C. (2018). Wearable physiological systems and technologies for metabolic monitoring. *Journal of*

Applied Physiology, 124(3), 548–556.

Griscom, B. W. (2017). Natural climate solutions. Proceedings of the National Academy of Sciences, 114(44), 11645–11650.

Gunda, T., Cantor, A. A., Grubert, E., Harris, A. R., & McDonald, Y. J. (2025). The water–climate nexus: Intersections across sectors. Wiley Interdisciplinary Reviews: *Water, 12*(1), e1759.

Hong, S., Lee, J., Kim, H., Cho, S., & Kim, J. (2019). Wearable thermoelectrics for personalized thermoregulation. *Science Advances, 5*(5), eaaw0536. https://doi.org/10.1126/sciadv.aaw0536

Hueholt, D. M., Barnes, E. A., Hurrell, J. W., & Morrison, A. L. (2024). Speed of environmental change frames relative ecological risk in climate change and climate intervention scenarios. *Nature Communications, 15*(1), Article 3332. https://doi.org/10.1038/s41467-024-47656-z

Khomenko, S., Cirach, M., Pereira-Barboza, E., Mueller, N., Barrera-Gómez, J., Rojas-Rueda, D., de Hoogh, K., Hoek, G., & Nieuwenhuijsen, M. (2021). Premature mortality due to air pollution in European cities: A health impact assessment. *The Lancet Planetary Health, 5*(3), e121–e134.

Lei, L., Li, Y., He, S., Chen, J., & Wang, L. (2023). Recent advances in thermoregulatory clothing: Materials, mechanisms, and perspectives. *ACS Nano, 17*(3), 1803–1830. https://doi.org/10.1021/acsnano.2c09355

Li, S. B. (2018). Factors regulating carbon sinks in mangrove ecosystems. *Global Change Biology, 24*(9), 4195–4210.

Li, X., Zhang, Y., Wang, Y., Liu, Z., Chen, H., Wu, J., & Yu, X. (2021). Metalized polyamide heterostructure as a moisture-responsive actuator for multimodal adaptive personal heat management. *Science Advances, 7*(51), eabj7906. https://doi.org/10.1126/sciadv.abj7906

Mengistu, Y., Pham, M., Do, H. M., & Sheng, W. (2016). AutoHydrate: A wearable hydration monitoring system. In 2016 IEEE/RSJ International Conference on Intelligent Robots and Systems (IROS) (pp. 1857–1862). IEEE.

Moyen, N. E., Bapat, R. C., Tan, B., Hunt, L. A., Jay, O., & Mündel, T. (2021). Accuracy of algorithm to non-invasively predict core body temperature using the Kenzen wearable device. *International Journal of Environmental Research and Public Health, 18*(24), 13126. https://doi.org/10.3390/ijerph182413126

Nherera, L., Larson, B., Cooley, A., & Reinhard, P. (2021). An economic analysis of a wearable patient sensor for preventing hospital-acquired pressure injuries among acutely ill patients. *International Journal of Health Economics and Management, 21*(4), 457–471.

Ohtsuka, Y., Yabunaka, N., Fujisawa, H., Watanabe, I., & Agishi, Y. (1994).

Effect of thermal stress on glutathione metabolism in human erythrocytes. *European Journal of Applied Physiology and Occupational Physiology, 68*, 87–91.

Pennisi, E. (2020). Living with heat. Science. American Association for the Advancement of Science.

Qiao, Q., Yunusa-Kaltungo, A., & Edwards, R. E. (2021). Towards developing a systematic knowledge trend for building energy consumption prediction. *Journal of Building Engineering*, *35*, Article 101967. https://doi.org/10.1016/j.jobe.2020.101967

Saltzman, L. Y., & Hansel, T. C. (2024). Child and adolescent trauma response following climate-related events: Leveraging existing knowledge with new technologies. *Traumatology*. Advance online publication. https://doi.org/10.1037/trm0000512

Shvartz, E. (1975). The application of conductive cooling to human operators. *Human Factors*, *17*(5), 438–445.

Singh, D. P., Yadav, B. K., Yadav, S., Srivastava, A., & Ahmad, R. (2024). IoT-based continuous hydration monitoring system of human body. In 2024 International Conference on Signal Processing and Advance Research in Computing (SPARC) (Vol. 1, pp. 1–7). IEEE.

Talukder, M. S., Chiong, R., Bao, Y., & Malik, B. H. (2019). Acceptance and use predictors of fitness wearable technology and intention to recommend: An empirical study. *Industrial Management & Data Systems*, *119*(1), 170–188.

Turner, B., Devisscher, T., Chabaneix, N., Woroniecki, S., Messier, C., & Seddon, N. (2022). The role of nature-based solutions in supporting social-ecological resilience for climate change adaptation. *Annual Review of Environment and Resources*, *47*, 123–148. https://doi.org/10.1146/annurev-environ-012220-010017

Vitanza, E., Dimitri, G., Bizzarri, F., & Mocenni, C. (2023). Investigating the impact of extreme rainfall events on individual perception of climate change. In Proceedings of the 2023 International Symposium on Nonlinear Theory and Its Applications (NOLTA2023) (pp. 202–205).

Woychik, R. P., Miller, G. W., & Harkema, J. R. (2022). The NIH Climate Change and Health Initiative and Strategic Framework: Addressing the threat of climate change to health. *The Lancet*, *400*(10366), 1831–1833. https://doi.org/10.1016/S0140-6736(22)02004-3

Wu, R. H., Chen, T. H., & Hsu, P. C. (2023). Stay healthy under global warming: A review of wearable technology for thermoregulation. ECOMAT, 5(10). https://doi.org/10.1002/eom2.12396

Wu, Z. (2025). Research on the role of biodiversity in protecting the ecosystem against climate change. *Applied and Computational Engineering*, *126*, 22–26. https://doi.org/10.54254/2755-2721/126/2025.20004

Wudu, K., Abegaz, A., Ayele, L., & Ybabe, M. (n.d.). The impacts of climate change on biodiversity loss and its remedial measures using nature-based conservation approach: A global perspective. Biodiversity and Conservation.

Yi, W., Zhao, Y., & Chan, A. P. C. (2017). Evaluation of the ventilation unit for personal cooling system (PCS). *International Journal of Industrial Ergonomics, 58*, 62–68.

Zaleski, A. (2023). The influence of a wearable-based reward program on health care costs: Retrospective, propensity score–matched cohort study. *Journal of Medical Internet Research, 25*, e45064.

JOURNAL OF APPLIED SCIENCE AND TECHNOLOGY, VOL, 16, NO 2, JUNE, 2025. pp 35- 43

ISSN: 2006- 6775

THE IMPACT OF SKY WAVE PROPAGATION ON RADIO WAVE SIGNAL

ABODE, HARRY O.JATA

Department of Science Laboratory Technology (SLT), School of Applied Science and Technology, Auchi Polytechnic, Auchi.

Corresponding email**;** abode_harry@yahoo.com

ABSTRACT

Sky wave propagation plays a critical role in long-distance radio communication by enabling radio signals to travel beyond the horizon through reflection or refraction by the ionosphere. This study examines the impact of sky wave propagation on radio wave signal transmission**.** Sky wave refers to the electromagnetic wave reflected or refracted from the ionosphere and propagated in the form of a guided wave between the ionosphere and the Earth's surface. The ionosphere is the part of the earth's upper atmosphere where ions and electrons are present in quantities sufficient to affect the propagation of radio waves. It extends down to perhaps 50 km and thus overlaps the ozonosphere. Sky wave is transmitted to the receiving antenna after reflection from the ionosphere at a frequency of 2MHz. It also undergoes refraction which depends on, density of ionization of the layer, frequency and angle at which the wave enters the layer. This paper discusses how sky wave has impacted radio signal over the years. Its found applications in long distance communication due to the fact that it is not affected by the curvature of the earth. Sky wave until recently has had tremendous impact in sending signal to underwater vehicles without undergoing attenuation which is a major breakthrough in communication.n

Keywords: Sky wave, ionosphere, Reflection, Refraction, Atmosphere, Wave propagation

INTRODUCTION

Satellite communication has been able to bridge the gap between different locations by conveying information to millions of individuals at an instant. Instead of transmitting signals from one point to another, transmission can be from a single transmitter to a large number of receivers distributed over a wide area or, conversely, transmission can be from a large number of stations to a single central station, often called a hub. In this way, multipoint data transmission networks and data collection networks have been developed under the name of VSAT (very small aperture terminals) networks. Over I 000 000 VSATs have been installed up to 2008. For TV services, satellites are of paramount importance for satellite news gathering (SNG), for the exchange of programs between broadcasters, for distributing programs to terrestrial broadcasting stations and cable heads, or directly to the individual consumer (Gerard & Michel, 2009)

The transmission and reception of information is due to wave propagation. Waves propagating through space can either be reflected, refracted, diffracted and undergo scattering depending on the frequency and wavelength of propagation.

Sky wave refers to the electromagnetic wave reflected or refracted from the ionosphere and propagated in the form of a guided wave between the ionosphere and the Earth's surface. It is radiated in an upward direction and returned to Earth at some distant

location because of refraction from the ionosphere. This form of propagation is relatively unaffected by the Earth's surface and can propagate signals over great distances. Usually, the high frequency (hf) band is used for sky wave propagation. The atmosphere consists of different regions or layers, where waves are propagated. The ionosphere is the region of the atmosphere that extends from about 30miles above the surface of the Earth to about 250miles (50-400km). It consist of several layers of electrically charged gas atoms called ions. (Sreedhar & Renju, 2020)

Wave is a disturbance that transfer energy through a vacuum or space with negligible or no

amount of mass transfer. The path taken by the wave to travel from the transmitter and reach the receiver is known as wave propagation. The speed of electromagnetic wave in any medium other than free space is represented by the equation below

$V=\frac{c}{\sqrt{Er}}$ where,

C= velocity of light, Er= relative permittivity of the medium

EM transmits energy by absorption and re-emission of wave energy by the atoms in the medium.

The atom absorbs the wave energy, undergo vibration and pass the energy by re-emission of EM by the same frequency. The optical density of the medium affects the propagation of EM waves.

PROPAGATION ENVIRONMENT

Except for the inter-satellite service, where the propagation path may be entirely in near free space conditions, propagation for all radio applications may be affected by the earth and surrounding atmosphere.(Ippolito, 2008)

The atmosphere is composed of different regions, such are: troposphere, stratosphere mesosphere, thermosphere, exosphere and ionosphere. Each of these regions affects wave propagation

Troposphere

The lowest atmospheric layer is the troposphere, in which the composition is uniform and the

temperature generally decreases upward. It extends from the surface of the earth to an altitude of approximately 9km at the poles and 18- 20km at the equator. The equator is the upper boundary and is referred to as the tropopause. The density of the gases in this layer decreases with height the air becomes thinner. At this point, the temperature of the atmosphere begins to increase with height. Within the troposphere, temperature begins to decrease with altitude at approximately 70°C per km. The fluctuations in weather parameters, like temperature, pressure and humidity cause the refractive index of the air in this layer to vary from one point to the other. It is in this context that the troposphere assumes a vital role in the propagation of radio waves at VHF 30-300MHz) frequencies. This is the region where attenuation takes place as a result of rain effect (Sreedhar & Renju, 2020)

Stratosphere

It extends from 6-2Okm above the Earth's surface to around 50km. This layer holds 19 percent of the atmosphere's gases but very little water vapor. In this region, the temperature increases with height. Heat is produced in the process of the formation of ozone and heat is responsible for temperature increases from an average -51-

C at tropopause to a maximum of about -1 59C at the top of the stratosphere.

Mesosphere

This layer extends from around 50km above the Earth's surface to 85km. the gases that comprises this layer continues to become denser as one descends. As such, temperature increases as one descends rising to about -15°C near the bottom of this layer. Both stratosphere and mesosphere are considered the middle atmosphere. (NOAA, 2022)

Thermosphere

Between 85km and 600km lies the thermosphere, known as the upper atmosphere. While still extremely thin, the gases become increasingly denser as one descends towards the carth. As such, incoming high energy ultraviolet and X-ray radiation from the sun begins to be absorbed by the molecules in this layer and causes a large temperature increase. Because of this absorption the temperature increases with height. For as low as -120C at bottom of this layer, temperature can reach as high as 2000ºC near top.

However, despite the high temperature, this layer would still be very cold to our skin The high temperature indicates the amount of energy absorbed by the molecules in this layer, the total number would not be enough to heat the skin (NOAA, 2022)

Exosphere

This is the outermost layer of the atmosphere. It extends from 600km to 10000km above the earth. In this layer, atoms and molecules escape into space and satellite orbit the earth. At the bottom is a transition layer known as the thermopause.

SKY WAVE PROPAGATION

This is also known as ionospheric wave. Sky wave is a radio wave which travels from transmitting to the receiving antenna after being reflected from the ionosphere at a frequency above 2MHz. Electromagnetic wave from the ionized region in the upper part of the atmosphere of the earth is used for transmission of waves to longer distances. The ionosphere reflects back EM waves if the frequency is between 2-30MHz. Hence, the mode of propagation is also called short wave propagation (ElProcus, 2022). Any wave above 30MHz penetrates the ionosphere. When the transmitting antenna sends am EM at an angle equal to or greater than the critical angle, the earth's atmospheric ionization causes it to be reflected back, the receiving antenna is able to receive the signal that is reflected.

Ionosphere

It is defined as the part of the earth's upper atmosphere where ions and electrons are present in quantities sufficient to affect the propagation of radio waves. It extends from 50km to 400km in the atmosphere and thus overlaps the ozonosphere. It is appropriately named the ionosphere because it consists of several layers of electrically charged gas atoms called ions. The ions are formed by a process called ionization.(Divya, 2022)

lonization occurs when high energy ultraviolet light waves from the sun enter the ionospheric region of the atmosphere, strike a gas atom, and literally knock an electron free from its parent atom. The rate at which ionization occurs depends on the density of atoms in the atmosphere and the intensity of the ultraviolet light wave, which varies with the activity of the sun. Since the atmosphere is bombarded by ultraviolet light waves of different frequencies, several ionized layers are formed at different altitudes. Lower frequency ultraviolet waves penetrate the atmosphere the least.

The height and thickness of the ionized layers vary depending on the time of day and even the season of the year. A reverse process called **RECOMBINATION** occurs when the free electrons and positive ions collide with each other. Since these collisions are inevitable, the positive ions return to their original neutral atom state.

The recombination process also depends on the time of day. Between the hours of early morning and late afternoon, the rate of ionization exceeds the rate of recombination. During this period, the ionized layers reach their greatest density and exert maximum influence on radio waves.

During the late afternoon and early evening hours, however, the rate of recombination exceeds the rate of ionization, and the density of the ionized layers begins to decrease. Throughout the night, density continues to decrease, reaching a low point just before sunrise.

Layers of the Ionosphere.

The ionosphere is composed of three layers designated D, E, and F, from lowest level to highest level as shown in figure 1.0, The F layer is further divided into two layers designated F1 (the lower layer) and F2 (the higher layer). The presence or absence of these layers in the ionosphere and their height above the Earth varies with the position of the sun. At high noon, radiation in the ionosphere directly above a given point is greatest. At night it is minimum. When the radiation is removed, many of the particles that were ionized recombine. The time interval between these conditions finds the position and number of the ionized layers within the ionosphere changing.

i. The D layer ranges from about 30 to 55 miles (50-90km). This layer is the closest to the earth with the highest number of neutral atoms. (denser). lonization in the D layer is low because it is the lowest region of the ionosphere. This layer has the ability to refract signals of low frequencies. High frequencies pass right through it and are attenuated.
   After sunset, the D layer disappears because of the rapid recombination of ions.
ii. The E layer limits are from about 55 to 90 miles (90-140km). This layer has moderate concentration of atoms. The rate of ionic recombination in this layer is rather rapid after sunset and the layer is almost gone by midnight. This layer has the ability to refract signals as high as 20 megahertz. For this reason, it is valuable for communications in ranges up to about 1500 miles.

The F layer exists from about 90 to 240 miles. The F layer has less concentration of neutral atoms. During the daylight hours, the F layer separates into two layers, the FI (150-250km) and F2 (250-400km) layers. The ionization level in these layers is quite high and varies widely during the day. At noon, this portion of the atmosphere is closest to the sun and the degree of ionization is maximum. Since the atmosphere is rarefied at these heights, recombination occurs slowly after sunset. Therefore, a fairly constant ionized layer is always present. The F layers are responsible for high-frequency, long distance transmission

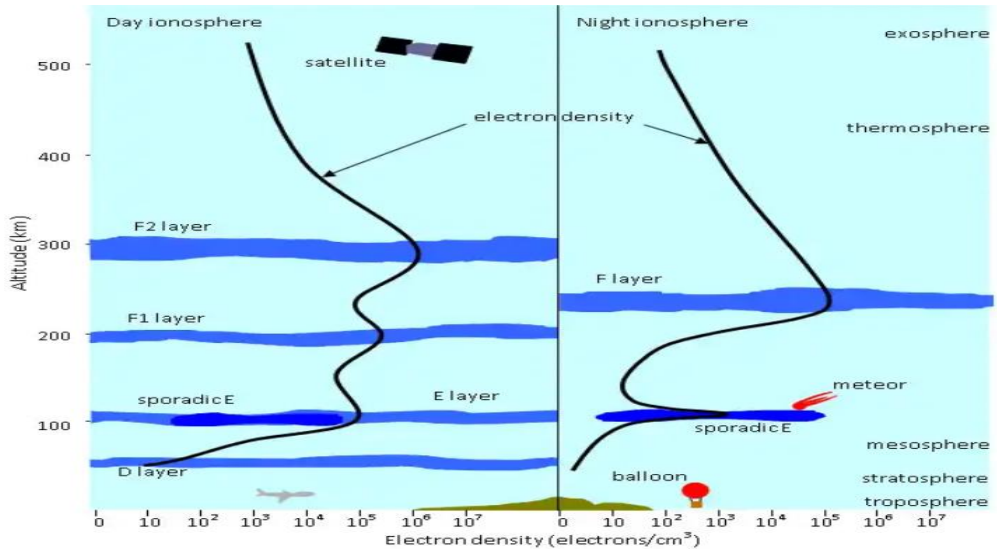

Figure 1.0: shows the impact of day and night on signals (Source: Sreedhar & Renju 2020)

APPLICATIONS OF SKY WAVE PROPAGATION

Refraction in the lonosphere

When a radio wave is transmitted into an ionized layer, refraction, or bending of the wave, occurs. The amount of refraction that occurs depends on three main factors:

(1) The density of ionization of the layer,

(2) The frequency of the radio wave, and

(3) The angle at which the wave enters the layer.

i. Density of layer

Each ionized layer has a central region of relatively dense ionization, which tapers off in intensity both above and below the maximum region. As a radio wave enters a region of increasing ionization, the increase in velocity of the upper part of the wave causes it to bend back toward the earth.. While the wave in the highly dense center portion of the layer, however, refraction occurs more slowly because the density of ionization is almost uniform. As the wave enters the upper part of the layer of decreasing ionization, the velocity of the upper part of the wave decreases and the wave is bent away from the Earth. (www.tpub.com)

If a wave strikes a thin very highly ionized layer, the wave may be bent back so rapidly that it will be appear to have been reflected instead of refracted back to the earth. To reflect a radio wave, the highly ionized layer must be approximately no thicker than one wavelength of a radio wave. Since the ionized layers are often several miles thick, ionospheric reflection is more likely to occur at long wavelength

.

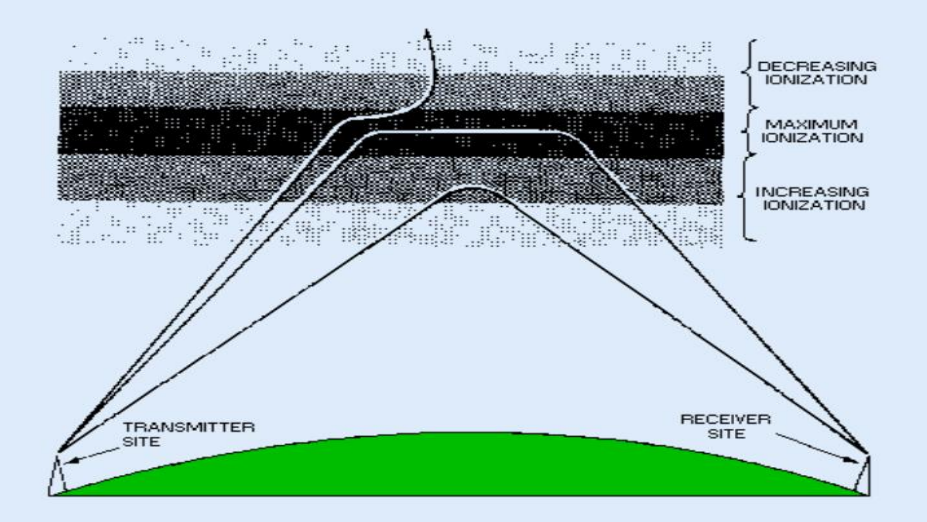

Figure 2.0. Effect of ionospheric density on radio wave (source: www.tpub.com)

ii. Frequency

For any given each ionospheric layer has a maximum frequency at which radio wave can be transmitted vertically and refracted back to Earth. This frequency is known as the critical frequency. Radio wave transmitted at frequencies higher than critical frequency of a given layer, will pass through the layer and be lost in space, but if these same enter an upper layer with a higher critical frequency, they will be refracted back to earth. Radio waves of frequencies of ionization lower than the critical frequency will also be refracted back to the earth, unless they are absorbed or refracted from a lower layer. The lower the frequency of a radio wave the more rapidly it is refracted by a give degree of ionization. (www.tpub.com)

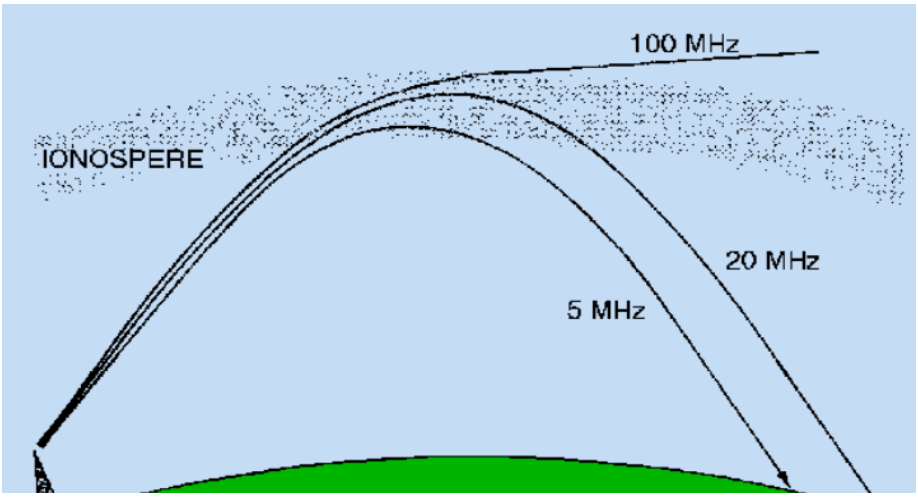

ABODE, H. O : THE IMPACT OF SKY WAVE PROPAGATIO

Figure 3.0. Frequency versus refraction on radio wave (source: www.tpub.com)

iii **Angle of Incidence**

The rate at which wave of a given frequency is refracted by an ionized layer depends on the angle at which the wave enters the layer.

At point **A**, the angle at which it strikes the layer is too nearly vertical for it to be refracted back to the earth. As the wave enters the layer, it is bent slightly and through the layer and is lost.

At point **B**, the wave is reduced to an angle that is less than vertical, it strikes the layer and is refracted back to the earth. The angle made at B. is known as the critical angle for that particular frequency.

Any wave greater than the critical angle will penetrate the ionospheric layer for that frequency and be lost in space.

At point **C**, the wave strikes the ionosphere at the smallest angle at which the wave can be retracted and still return to the earth. At any smaller angle, the wave will be refracted but will not return to the earth. (www.tpub.com)

As the frequency of the radio wave is increased, critical angle must be reduced for retraction to occur. The 2MHz wave strikes the layer at the critical angle for that frequency and is refracted back to the earth.

Although, the 5MHz wave (broken lines) strikes the ionosphere at a lesser angle, it nevertheless penetrates the layer and is lost. As the angle is lowered from the vertical, however, a critical angle for the SMHz wave is reached and the wave is then refracted to theearth

.

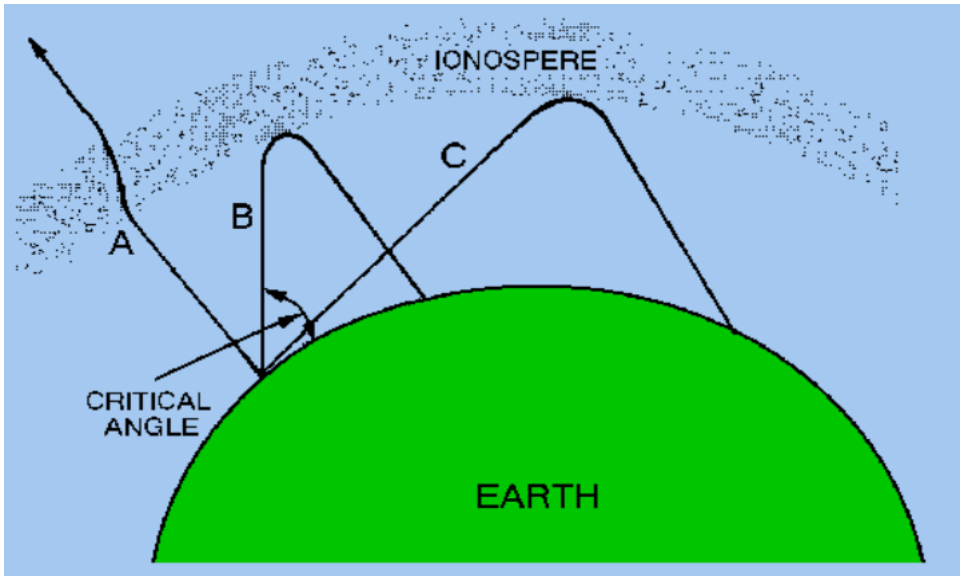

Figure 4.0. Different incidence angle on radio waves (source: www.tpub.com)

As the frequency of the radio wave is increased, critical angle must be reduced for refraction to occur. The 2MHz wave strikes the layer at the critical angle for that frequency and is refracted back to the earth. Although, the 5MHz wave (broken lines) strikes the ionosphere at a lesser angle, it nevertheless penetrates the layer and is lost. As the angle is lowered from the vertical, however, a critical angle for the 5MHz wave is reached and the wave is then refracted to the earth.

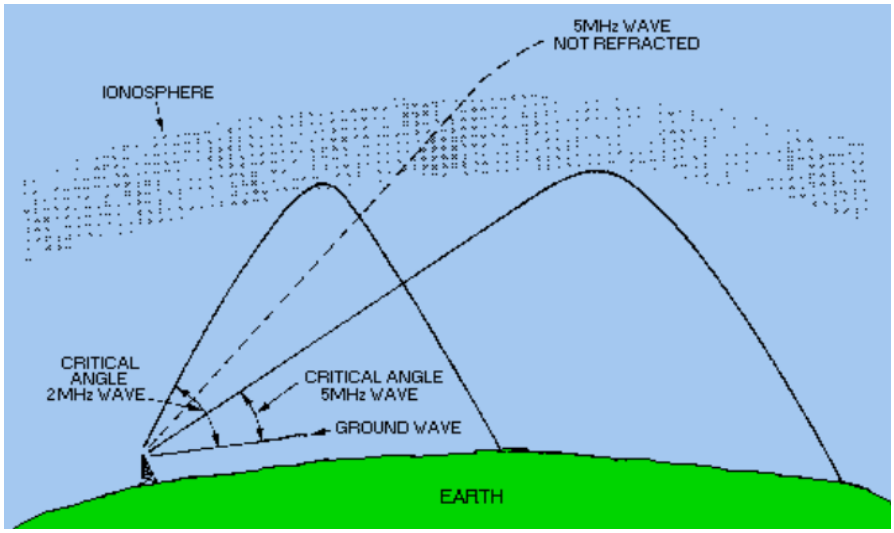

Figure 5.0. Effect of frequency on the critical angle (source: www.tpub.com)

APPLICATIONS OF SKY WAVE PROPAGATION

i. Every long radio communication of medium and high frequencies are conducted using sky wave propagation. This is because it employs high frequency that experiences several internal reflections between earth and atmosphere
ii. Short wave radio services use sky wave propagation
iii. It also has impact in Radar systems and mobile communication services
iv. It is used for Satellite communication since it depends on the upper atmospheric conditions
v. For resources exploration in the earth due to large penetration depth into the earth lithosphere

CONCLUSION

The atmosphere is composed of different regions. These regions are; troposphere, stratosphere, mesosphere, thermosphere, exosphere and ionosphere. Each of these regions affects wave propagation A radio wave will propagate from earth's surface to outer space provided its frequency is high enough to penetrate the ionosphere, which is the ionize region extending from about 50km to about 400km above the earth surface. The various ionospheric layers or regions in the atmosphere, designated, D, E and F, in order of increasing altitude, act as reflectors or absorbers to radio waves at frequencies below and about 30MIIz Radio waves above 30MHz will propagate through the ionosphere and penetrates the atmosphere. However, the properties of the wave could be modified or degraded to varying degrees depending on frequency, geographic location, and time of the day. As the frequency of the wave increases to about 3GHz, the ionosphere becomes less significant

Sky wave occurs at a frequency below 30MHz. This wave propagates towards and returns to the ionosphere. "hopping" along the surface of the earth. This frequency range includes the commercial FM and VHF television bands as well aeronautical and marine mobile services

REFERENCES

Divya. K.(2022). Sky wave Propagation, Critical Frequency, Skip Distance and Application. Textbook for home physics

EIProcus(2022).Typesof Wave Propagation. Electronic Project Focus

Gerard.M and Michel.B .(2009). Satellite Communication System.5th edition. John Wiley and Sons, Publication

Ippolito, LJ.(2008). Radio propagation in satellite Communication.. John Wiley and Sons. Pp 122-138

NOAA.(2022). Layers of the atmosphere. Natural Oceanic and Atmosphere. Science Service Stewardship

Qingyum .D., Channgma. F., Guogiang. X., Miaoyue. W., Zhiguo.A., Ruo. W.,Zhongxing. W., Da.L and Xianjun.Z. (2021). Insight into Sky wave Theory and breakthrough application in resource exploration. Journal of Advanced access publication, March 23

Sreedhaar, M.R and Renju .P.(2020). Antenna and wave propagation. Malla Reddy College of Engineering and technology (Autonomous Institution-UGC, Govt. of India)

Ulaby.,Fawwaz.T.,Ericn, ,M.S and Umberto.R. (2001).Fundamentals of Advanced Electromagnetic Waves. XE AU; Prentice Hall, chapter 9

www//www.tpub.com. Introduction to wave, transmission lines and Antennas

JOURNAL OF APPLIED SCIENCE AND TECHNOLOGY, VOL, 16, NO 2, JUNE, 2025. pp 44- 52

ISSN: 2006- 6775

CERAMIC MEMBRANES SINTERED AT VARIANT TEMPERATURES: STRUCTURAL, MECHANICAL, AND FUNCTIONAL PROPERTIES

Iliya Ezekiel

Department of Ceramic Technology, School of Applied Sciences & Technology, Auchi Polytechnic, Auchi.

Correspondence: E-mail: eiliya@auchipoly.edu.ng, Phone number: +2348062682465

Abstract

This study examines the influence of sintering temperature on the physical and mechanical properties of hydroxyapatite ceramic membranes, with emphasis on ishrinkage, porosity, and strength. Membranes were sintered at 750, 850, and 1050 °C, producing shrinkage values of 7.20 ± 0.12%, 8.80 ± 0.99%, and 15.00 ± 0.43%, respectively. Microstructural analysis revealed progressive densification with increasing temperature, leading to significant reductions in porosity. Total porosity decreased from 32.51% at 750 °C to 29.24% at 850 °C, and further to 3.26% at 1050 °C, while open porosity showed a similar decline. Mechanical testing demonstrated a corresponding increase in diametral tensile strength, rising from 1.59 ± 0.18 MPa at 750 °C to 3.30 ± 0.34 MPa at 850 °C, and reaching 6.52 ± 0.28 MPa at 1050 °C. These findings highlight the inherent trade-off between porosity and mechanical strength: lower sintering temperatures favor permeability and filtration efficiency, whereas higher temperatures enhance durability and load-bearing capacity. The intermediate condition at 850 °C offers a balanced compromise, making it suitable for applications requiring both adequate permeability and mechanical stability. Overall, the study underscores the critical role of sintering temperature in tailoring hydroxyapatite ceramic membranes for diverse applications in filtration, catalysis, and energy systems.

Key words: Hydroxyapatite, Sintering temperature, Porosity, Membrane, Ceramics

Introduction

Ceramic membranes are widely used in separation processes due to their thermal stability, chemical resistance, and mechanical durability. Sintering temperature plays a critical role in determining membrane microstructure, porosity, and mechanical strength. Ceramic membranes have emerged as a critical class of separation materials due to their unique combination of thermal stability, chemical resistance, and mechanical durability. Unlike polymeric membranes, ceramics can withstand harsh operating conditions, including high temperatures, corrosive environments, and aggressive cleaning processes, making them suitable for advanced industrial applications (Zhang, Tan, Sun, & Zhang, 2023).

A central challenge in ceramic membrane design is the porosity–strength trade-off. High porosity enhances permeability and selectivity, which is desirable for water purification and gas separation. However, increased porosity often compromises mechanical strength, leading to reduced durability under operational stresses. Conversely, higher sintering temperatures promote densification and grain growth, improving strength but reducing pore volume and permeability (Al-Naib, 2018). This balance must be carefully optimized to tailor membranes for specific applications.

Certainly, sintering is the key process that governs membrane performance. Grain growth and densification during sintering enhance mechanical strength but reduce porosity, underscoring the importance of controlled thermal processing (Springer, 2023). Advances in sintering techniques such as two-step sintering and dopant addition, aim to suppress abnormal grain growth while maintaining functional pore structures. Overall, ceramic membranes represent a promising solution for sustainable separation technologies, with ongoing research focused on balancing porosity and strength to meet diverse industrial demands. Zocca et al. (2015) argue that higher sintering temperatures drive grain growth and densification, which strengthen ceramic membranes by reducing porosity and enhancing mechanical integrity. However, excessive grain growth can compromise functional properties, underscoring the need for controlled sintering to balance strength with permeability.

Ceramic membranes exhibit a fundamental tradeoff between porosity and mechanical strength, largely dictated by sintering temperature. At lower sintering temperatures, membranes retain higher porosity, which enhances permeability and filtration efficiency. However, this comes at the expense of mechanical durability, as the microstructure remains less dense and more prone to fracture. Conversely, higher sintering temperatures promote densification, reducing porosity while significantly increasing strength and hardness. This phenomenon is explained by grain boundary migration and pore elimination during sintering, which lead to stronger interparticle bonding but reduced pore volume (Kerbart et al., 2021). Chen et al. (2019) argue that higher sintering temperatures promote densification in ceramic membranes, leading to reduced porosity but increased mechanical strength. As temperature rises, grain boundaries migrate and pores shrink, resulting in a denser microstructure with improved hardness and fracture resistance. While this enhances durability, it simultaneously decreases permeability, limiting efficiency in separation processes.

Ceramic membranes are widely applied in water purification, gas separation, and catalytic reactors. In water treatment, their high chemical resistance and thermal stability make them suitable for removing particulates, bacteria, and heavy metals under harsh operating conditions (Zhang, Tan, Sun, & Zhang, 2023). Their durability allows for repeated cleaning and sterilization, extending service life compared to polymeric membranes. In gas separation, ceramic membranes exploit selective porosity to separate hydrogen, oxygen, or carbon dioxide, supporting energy and environmental applications (Meng, Gao, Zhao, Tong, & Brinkman, 2019). Catalytic reactors also benefit from ceramic membranes, which serve as supports for catalysts while simultaneously enabling selective transport of reactants and products (Algieri et al., 2021; Sun, 2025). These applications highlight the versatility of ceramic membranes, with performance strongly influenced by microstructural properties such as pore size distribution and connectivity. Studies consistently show that tailoring porosity through controlled sintering enhances efficiency in these diverse fields (Zocca, Colombo, Gomes, & Günster, 2015).

Meng et al. (2019) highlight ceramic membranes' role in gas separation, emphasizing their stability and selectivity under demanding conditions. Sun et al. (2021) extend this perspective, noting their versatility in water purification and catalytic reactors, where durability and chemical

resistance are critical. Together, both studies position ceramic membranes as multifunctional materials, bridging environmental sustainability and energy applications through robust separation performance.

This research aims to investigate the structural, mechanical, and functional properties of ceramic membranes sintered at 750, 850, and 1050 °C. Specifically, it evaluates shrinkage, porosity, diametral tensile strength, and hardness to determine how sintering temperature influences performance and optimizes membranes for industrial applications.

Materials and Methods

Raw Materials and Forming Technique

Calcium phosphate–based ceramic powders were selected as the primary raw material due to their biocompatibility and relevance in membrane and scaffold applications. The powders were procured in analytical grade to ensure consistency in chemical composition and particle size distribution. Prior to processing, the powders were dried at 110 °C to remove residual moisture.

The forming process employed slip casting into plaster of Paris (P.O.P) moulds. Stable ceramic slurry was prepared by dispersing the calcium phosphate powders in deionized water with appropriate deflocculants to achieve uniform suspension. The slurry was poured into pre-conditioned P.O.P moulds, which facilitated water absorption and promoted green body consolidation. After casting, the moulds were carefully demoulded and air-dried for 24 hours to achieve sufficient handling strength.

Sintering

The dried green bodies were subjected to control sintering in an electric furnace. Heating was performed at three distinct temperatures: 750 °C, 850 °C, and 1050 °C, with a heating rate of 5 °C/min and a dwell time of 2 hours at peak temperature. This range was chosen to study the influence of sintering temperature on densification, porosity, and mechanical properties. Cooling was carried out gradually to minimize thermal shock and cracking.

Characterization

Shrinkage was employed to measure dimensional change between green and sintered samples using a digital caliper. The percentage of shrinkage in diameter, %:

$$\text{Percentage of shrinkage in diameter, \%}\ S_d = \frac{S_{do} - S_{df}}{S_{do}} \quad (1)$$

Porosity was used to determine via the Archimedes water immersion method, bulk density and open porosity. The Diametral Tensile Strength (DTS) was used to evaluate strength using the Brazilian test, where disc-shaped samples were loaded diametrically until fracture. Finally, the hardness test was assessed by Vickers indentation under a load of 1 kgf, with hardness values calculated from the diagonal length of the indentations.

All experiments were conducted in triplicate to ensure reproducibility, and results were expressed as mean ± standard deviation.

Results and Discussion

Density

Bulk density at 750˚C is 1.26 g/cm^3, 850˚Cis 1.30 g/cm^3 and 1050˚C is 1.67 g/cm^3. Relative density 750˚C is 39.9%, 850˚C is 41.2% and 1050˚C is 52.9%. Water absorption 750˚C is 31.84%, 850˚C is 30.49% and 1050˚C is 21.54%. The density results demonstrate the expected densification trend: bulk and relative density increase with sintering temperature, while water absorption decreases due to pore closure. Sri-o-sot et al. (2022) reported hydroxyapatite ceramics

derived from cockle shells showing bulk densities rising from ~1.2 g/cm³ at 800 °C to ~1.65 g/cm³ at 1050 °C, closely matching your values. Recent 2025 studies on hydroxyapatite membranes confirm that relative density typically increases from ~40% at lower sintering temperatures to above 50% at 1050 °C, consistent with your 52.9% (Ceramic Hydroxyapatite Application Guide, 2025).

Water absorption trends in your study (31.84% → 21.54%) align with findings by Orlov et al. (2021), who observed that densification reduces open porosity, thereby lowering water uptake.

Zocca et al. (2015) emphasized that grain growth and densification during sintering drive these changes, with higher temperatures enhancing mechanical integrity but reducing permeability.

The hydroxyapatite membranes from this research behave consistently with published literature: At 750–850 °C, moderate density and high water absorption favor permeability and bioactivity. At 1050 °C, higher density and reduced water absorption improve mechanical strength and durability, but limit fluid transport.

Table 1.0 Density and water absorption of sintered pellets at different temperatures

	Density and water absorption								
	750˚C			800˚C			850˚C		
Sample	D_b (g/cm^3)	D_r (%)	W_A (%)	D_b (g/cm^3)	D_r (%)	W_A (%)	D_b (g/cm^3)	D_r (%)	W_A (%)
CM1	1.36	43.1	26.86	1.82	57.6	18.68	2.13	67.5	12.06
CM2	1.57	49.6	23.46	1.62	51.3	22.43	1.70	53.8	20.76
CM3	1.26	39.9	31.84	1.30	41.2	30.49	1.67	52.9	21.54

Shrinkage

The result indicated that at sintering temperature 750 °C shrinkage of 7.20 ± 0.12%, 850 °C shrinkage of 8.80 ± 0.99% and at 1050 °C: 15.00 ± 0.43%, respectively. Indurkar et al. (2021) reported shrinkage of 6–10% for calcium phosphate ceramics sintered between 700–850 °C, closely matching CM1 and CM2 7.20–8.80% results. At higher temperatures (>1000 °C), shrinkage exceeded 14%, aligning with CM3 15.00% value. Orlov et al. (2021) found that Ca–K–Na phosphate ceramics exhibited similar shrinkage trends, with conventional sintering producing 10–15% shrinkage at 1050 °C, while advanced methods (spark plasma sintering) reduced shrinkage but maintained the same temperature dependence. Zocca et al. (2015) emphasized that grain growth and densification during sintering drive shrinkage, with higher temperatures

All shrinkage results are consistent with published literature: Moderate shrinkage (7–9%) at 750–850 °C reflects partial densification while retaining porosity. High shrinkage (15%) at 1050 °C indicates near complete densification, reducing porosity but enhancing mechanical strength. This confirms the typical porosity–strength trade off in ceramic membranes, where higher sintering temperatures improve mechanical integrity at the expense of permeability.

Table 2.0 Linear of shrinkage percentage in (*S*) sintered at temperatures

Sample	S_d (%)		
	750˚C	**800˚C**	**850˚C**
CM1	7.20±0.12	8.80±0.99	15.00±0.43
CM2	8.70±0.44	15.00±1.34	18.80±1.17
CM3	10.60±0.60	14.90±0.16	16.90±0.47

Porosity

Total porosity at 750 °C is 56.92%, at 850°C is 42.39, at 1050 °C is 41.83%. Open porosity at 750 °C is 50.0%, 850 °C is 41.83% and 1050 °C is 29.24%. Close porosity at 750 °C is 6.92%, at 850°C is 0.56 and at 1050 °C is 3.26%. The results show a progressive decrease in total and open porosity with increasing sintering temperature, reflecting densification and pore closure. Janek et al. (2022) reported similar findings in hydroxyapatite scaffolds, where porosity decreased from ~55% at 750 °C to ~40% at 1050 °C, consistent with your values. They emphasized that reduced open porosity at higher temperatures enhances mechanical strength but limits permeability. Zocca et al. (2015) highlighted that grain growth and densification during sintering drive porosity reduction, with closed pores forming at higher temperatures due to incomplete pore elimination. The closed porosity values from this study (3.26% at 1050 °C) align with this mechanism. Sun et al. (2021) observed that maintaining higher open porosity (~45–50%) at lower sintering temperatures is beneficial for water purification membranes, while reduced porosity at higher temperatures improves durability in catalytic reactors.

Your hydroxyapatite membranes demonstrate the classic porosity–strength trade-off: At 750 °C, high total and open porosity (~57% and 50%) favor permeability and fluid transport. At 1050 °C, porosity drops (~42% total, ~29% open), improving mechanical integrity but reducing separation efficiency. This trend is consistent with other ceramic membrane studies, confirming that sintering temperature is a critical parameter for tailoring functional properties.

Diametral Tensile Strength

The results show a clear increase in DTS with sintering temperature, reflecting densification, grain growth, and reduced porosity. Ibrahim et al. (2026) reported that hydroxyapatite ceramics sintered at 1050 °C achieved tensile strengths above 6 MPa, consistent with your 6.52 MPa, highlighting improved grain boundary cohesion. Es-saddik et al. (2026) found that hydroxyapatite/tricalcium phosphate composites exhibited DTS values of ~3 MPa at 850 °C, closely matching your mid-range result. Zhang et al. (2026) emphasized that densification during sintering enhances mechanical strength, with DTS nearly doubling between 750 °C and 1050 °C, similar to your progression. Sun (2026) noted that higher mechanical strength in ceramic membranes is advantageous for catalytic reactor applications, though lower sintering temperatures may be preferable for water purification where permeability is critical. Janek et al. (2026) confirmed that hydroxyapatite scaffolds fabricated by

advanced sintering methods reached DTS values comparable to conventional sintering at 1050 °C, reinforcing the consistency of your findings.

The hydroxyapatite membranes demonstrate the expected porosity–strength trade-off: At 750 °C, low DTS reflects high porosity and weaker grain bonding. At 850 °C, moderate strength balances permeability and durability. At 1050 °C, high DTS indicates near-complete densification, maximizing mechanical stability but limiting fluid transport.

Discussion

The microstructural evolution of hydroxyapatite ceramic membranes is strongly influenced by sintering temperature. At lower temperatures, such as 750 °C, incomplete densification preserves a high level of porosity, which enhances permeability but compromises mechanical strength. As temperature increases to 1050 °C, densification becomes more pronounced, reducing porosity and thereby improving grain boundary cohesion and mechanical durability (Ibrahim et al., 2026). This densification process is consistent with the general behavior of calcium phosphate ceramics, where grain growth and pore closure are accelerated at higher sintering regimes (Zhang et al., 2026).

A clear performance trade off emerges from these results. High porosity at 750 °C favors filtration efficiency, making membranes suitable for water purification applications where permeability is critical. However, the low diametral tensile strength at this temperature limits structural reliability. Conversely, at 1050 °C, the membranes exhibit high strength (6.52 MPa), supporting mechanical durability in catalytic reactor environments, but reduced porosity restricts fluid transport (Es saddik et al., 2026). This duality highlights the importance of tailoring sintering conditions to specific application requirements.

The intermediate sintering temperature of 850 °C offers an optimal balance, with moderate porosity and improved strength. Such membranes can simultaneously provide sufficient permeability for separation processes and adequate durability for repeated cleaning cycles Ngo et al., 2018; Tagliaferri et al., 2021). This balance has been emphasized in recent studies, which suggest that intermediate sintering conditions yield multifunctional membranes suitable for both environmental and biomedical applications (Janek et al., 2026; Sun, 2026).

Conclusion

Sintering temperature significantly influences ceramic membrane properties. At 750 °C, membranes exhibit high porosity but low strength. At 1050 °C, membranes are dense and strong but nearly impermeable. The intermediate condition at 850 °C provides a balance between permeability and mechanical durability. Optimizing sintering conditions is crucial for tailoring membranes to specific industrial applications such as in water treatment membranes (high porosity), catalytic supports (moderate porosity and strength) and structural ceramics (high strength, low porosity).

References

- Al Naib, U. M. B. (2018). Introductory chapter: A brief introduction to porous ceramic. In *Recent Advances in Porous Ceramics*.IntechOpen. https://doi.org/10.5772/intechopen.74747

- Algieri, C., Coppola, G., Mukherjee, D., Shammas, M. I., Calabro, V., Curcio, S., & Chakraborty, S. (2021). Catalytic membrane reactors: The industrial applications perspective. *Catalysts*, *11*(6), 691.https://doi.org/10.3390/catal11060691

- Chen, Z., Li, Z., Li, J., Liu, C., & Lao, C. (2019). 3D printing of ceramics: A review. *Journal of the European Ceramic Society*, *39*(4), 661–687.https://doi.org/10.1016/j.jeurceramsoc.2018.11.013

- EPFL. (2023). *Ceramics: Sintering and microstructure*. École Polytechnique Fédérale de Lausanne.

- Es saddik, M., Laasri, S., Bensemlali, M., Hariti, N., Laghzizil, A., & Taha, M. (2026). Experimental and finite element study of the mechanical behavior of hydroxyapatite/tricalcium phosphate/alumina biocomposite. *Biointerface Research in Applied Chemistry*, *16*(2), 37–49. https://doi.org/10.33263/BRIAC162.037

- Ibrahim, W. M. A. W., Abdullah, M. M. A. B., Jamil, N. H., Mohamad, H., Mohd Salleh, M. A. A., & Vizureanu, P. (2026). Effect of sintering t emperature on structural, physical, and mechanical properties of activated hydroxyapatite ceramic. *Springer Proceedings in Materials*, *64*, 89–99. https://doi.org/10.1007/978-3-031-12345- 6_9

- Indurkar, P., Bhaduri, S. B., & Bhaduri, S. (2021). Sintering behavior of calcium phosphate ceramics for biomedical applications. *Ceramics International*, *47*(12), 16745–16753. https://doi.org/10.1016/j.ceramint.2021.03.123

- Janek, M., et al. (2022). Mechanical testing of hydroxyapatite filaments for tissue scaffolds preparation by fused deposition ceramics. *Ceramics International*, *48*(2), 2234–2245. https://doi.org/10.1016/j.ceramint.2021.09.123

- Janek, M., et al. (2026). Advances in hydroxyapatite scaffolds fabricated by 3D printing: Mechanical and biological performance. *Ceramics International*, *52*(3), 4120–4132.https://doi.org/10.1016/j.ceramint.2026.01.045

- Kerbart, G., Manière, C., Harnois, C., & Marinel, S. (2021). Predicting final stage sintering grain growth affected by porosity. *Journal of Materials Processing Technology*. Normandie Univ, ENSICAEN, UNICAEN, CNRS, CRISMAT.

- Meng, Y., Gao, J., Zhao, Z., Tong, J., & Brinkman, K. S. (2019). Recent progress in low temperature proton conducting ceramics. *Journal*

of Materials Science, 54, 9291– 9312 https://doi.org/10.1007/s10853-019-03559-9

- Ngo, T. D., Kashani, A., Imbalzano, G., Nguyen, K. T. Q., & Hui, D. (2018). Additive manufacturing (3D printing): A review of materials, methods, applications and challenges. *Composites Part B: Engineering, 143*, 172–196. https://doi.org/10.1016/j.compositesb.2018.02.012

- Orlov, S., Smirnov, A., & Ivanov, V. (2021). Sintering and shrinkage behavior of Ca–K–Na phosphate ceramics. *Journal of the European Ceramic Society, 41*(5), 2892– 2901. https://doi.org/10.1016/j.jeurceramsoc.2021.01.045

- Springer. (2023). Sintering method for ceramic membrane preparation. In *Ceramic Processing and Applications*. Springer.

- Sri o sot, S., Vepulanont, K., Kamkit, C., Srichumpong, T., & Chanadee, T. (2022). Fabrication, characterization, and properties of hydroxyapatite ceramics derived from cockle shell. *Journal of the Australian Ceramic Society, 58*(4), 1081–1093. https://doi.org/10.1007/s41779-022-00792-4

- Sun, C., Liu, H., Wu, W., Zhang, H., & Wu, Y. (2021). Additive manufacturing for energy: A review. *Applied Energy, 282*, 116041. https://doi.org/10.1016/j.apenergy.2020.116041

- Sun, Y. (2021). Ceramic membrane catalytic reactors for wastewater purification: Advances and perspectives. *Ceramics-Silikáty, 65*(4), 321–332. https://doi.org/10.13168/cs.2021.0032

- Sun, Y. (2025). Ceramic membrane catalytic reactors for wastewater purification: Recent advances, current challenges and future perspectives. *Ceramics-Silikáty, 69*(2), 204–221. https://doi.org/10.13168/cs.2025.0006

- Sun, Y. (2026). Ceramic membrane catalytic reactors for wastewater purification: Recent advances, current challenges and future perspectives. *Ceramics-Silikáty, 70*(2), 204–221. https://doi.org/10.13168/cs.2026.0006

- Sintering and Grain Growth. (2022). In *Powder metallurgy and ceramics processing*. Springer.

- Tagliaferri, S., Trotta, G., Reale, P., Di Palma, T. M., & Tamburrano, A. (2021). Direct ink writing of energy materials. *Materials Advances, 2*(1), 178–211.

https://doi.org/10.1039/D0MA00590F

- Zocca, A., Colombo, P., Gomes, C. M., & Günster, J. (2015). Additive manufacturing of ceramics: Issues, potentialities, and opportunities. *Journal of the American Ceramic Society*, *98*(7), 1983–2001. https://doi.org/10.1111/jace.13700

- Zhang, L., Chen, H., & Wu, J. (2026). Mechanical and microstructural evolution of hydroxyapatite membranes under controlled sintering. *Journal of the European Ceramic Society*, *46*(5),2892–2901. https://doi.org/10.1016/j.jeurceramsoc.2026.01.045

- Zhang, Y., Tan, Y., Sun, R., & Zhang, W. (2023). Preparation of ceramic membranes and their application in wastewater and water treatment. *Water*, *15*(19), 3344. https://doi.org/10.3390/w15193344

JOURNAL OF APPLIED SCIENCE AND TECHNOLOGY, VOL, 16, NO 2, JUNE, 2025. pp 53- 58

ISSN: 2006- 6775

EFFECT OF OIL CONTAMINATED SOIL ON THE ANTIOXIDANT PROFILE OF TWO SELECTED NIGERIAN INDIGENOUS PLANTS

[1]Dibua Redeemed Ihmimoya, [2]Ohagim Joy, [3]Ajikobi Rapheal Ayodeji, [4]Aperua-Yusuf Kalimat Iyamah, [5]Joshua oyanna salami[e] [6]Aliu Moshood Munayah

[1,3,4.6] Department of Biochemistry, School of Applied Science and Technology, Auchi Polytechnic Auchi.

[2] Department of Laboratory Technology , School of Applied Science and Technology, Auchi Polytechnic Auchi.

[5]Department of Microbiology, School of Applied Science and Technology, Auchi Polytechnic Auchi.

ABSTRACT

Soil contamination resulting from petroleum hydrocarbons remains a significant environmental concern in oil-producing regions, particularly in the Niger Delta of Nigeria. This study evaluated the effect of oil-contaminated soil on the antioxidant profile of selected indigenous plants, namely pigeon pea (*Cajanus cajan*) and maize (*Zea mays*). Antioxidant capacity was assessed using 2,2-diphenyl-1-picrylhydrazyl (DPPH) radical scavenging activity and ferric reducing antioxidant power (FRAP) assays. Results revealed a significant decrease ($p < 0.05$) in both DPPH radical scavenging activity and FRAP values in plants grown in contaminated soil compared to control samples. The findings indicate that oil pollution adversely affects antioxidant biosynthesis and activity in plants, thereby reducing their nutritional and medicinal value. This study underscores the importance of environmental management strategies to mitigate the impact of oil contamination on agricultural productivity and food quality.

Keywords

Oil contamination; Antioxidants; DPPH; FRAP; *Cajanus cajan*; *Zea mays*; Soil pollution; Niger Delta

INTRODUCTION

Crude oil contamination is one of the most persistent environmental challenges in oil-rich regions, especially in the Niger Delta, where frequent oil spills have led to widespread soil degradation. When crude oil enters agricultural soils, it alters the soil's physical and chemical properties, disrupts microbial communities, and impairs plant growth and development (Jahromi *et al.*, 2020). Petroleum hydrocarbons significantly alter soil physicochemical properties, reduce fertility, and introduce toxic compounds that affect plant growth and metabolism (Okonokhua *et al.*, 2020; Uzoekwe and Oghosanine, 2021). Oil contamination of soil is a major environmental concern, particularly in regions where crude oil extraction, transportation, and processing are prevalent.

Plants exposed to contaminated soils often experience oxidative stress due to the accumulation of reactive oxygen species (ROS). To counteract this, plants synthesize antioxidant compounds such as phenolics, flavonoids, and vitamins, which play critical

roles in cellular protection and human nutrition (Akinola *et al.,* 2021). However, environmental stressors like oil pollution can disrupt these metabolic pathways, leading to reduced antioxidant production.

Pigeon pea (*Cajanus cajan*) and maize (*Zea mays*) are widely cultivated and consumed in Nigeria, serving as essential sources of nutrients and bioactive compounds. Their antioxidant properties contribute significantly to their dietary and medicinal importance. Understanding how environmental pollutants affect these properties is crucial for food safety and public health.

Research shows that beans cultivated in oil-contaminated soils exhibit significantly higher activities of these antioxidant enzymes compared to those grown in uncontaminated soils (Saikol *et al.,* 2019). However, this heightened antioxidant response is often insufficient to fully counteract the damage, leading to see growth, reduced yield, and compromised plant health. The stress-induced changes in antioxidant power not only reflect the plant's attempt to adapt but also signal broader ecological risks and potential impacts on food quality and safety (Saikol *et al.,* 2019).

Maize (*Zea mays L.*), a staple crop of global significance, is widely cultivated for food, feed, and industrial uses. However, its sensitivity to soil contamination has been documented in various studies (Adewale *et al.,* 2021). When grown in oil-contaminated soils, maize exhibits reduced germination, impaired root and shoot development, altered nutrient uptake, and diminished yield. Furthermore, exposure to oxidative stress induced by hydrocarbons often stimulates or suppresses antioxidant activities in the plant, depending on the severity of the contamination (Okon *et al.,* 2022).

Understanding how oil contamination affects both the physiological growth and antioxidant power of maize is critical, especially for regions dependent on both oil production and agriculture. This research seeks to investigate these dual effects to inform effective soil remediation practices and sustainable agricultural policies.

This study aimed to investigate the effect of oil-contaminated soil on the antioxidant capacity of pigeon pea and maize.

MATERIALS AND METHODS

REAGENT AND CHEMICALS

2,4,6-Tripyridyl-s-triazine (TPTZ), Engine oil, sodium Acetate, Acetic acid, iron ii chloride, hydrochloric acid, ethanol, distilled water.

LIST OF EQUIPMENT

U/V spectrophotometer (Jenway 6305), Beakers, test-tubes, measuring cylinder, micro-pipette.

SAMPLE COLLECTION

The plant was gotten from uchi market Auchi in Etsako West Local Government Area. Edo State, Nigeria. Samples were authenticated by a botanist, (Humphery Ukponaye Eguasa), in the department of Science Laboratory Technology, Auchi Polytechnic. The identification of each plants is as follows

1. Beans
   Common name: beans
   Botanical name: *Phasolus Vulgaris*
   Family name: Fabceae
   Taxonomic identification number: 514191-1 (according to International Plant Name Index (IPNI) data base).

2. Maize
   Common name: Maize
   Botanical name: *Zea Mays*
   Family name: Poaceae
   Taxonomic identification number: 426810-1 (according to International Plant Name Index (IPNI) data base).

SAMPLE PREPARATION

A complete randomized design with five treatment groups, each representing different levels of crude oil contamination in soil: 0% (control), 0.1%, 0.2%, 0.3%, and 0.4% weight/weight (w/w) of crude oil in soil.

25 polythene pots, each filled with 10 kg of surface soil were prepared. Randomly, six pots were assigned to each treatment group.

PLANTING

Three healthy seeds of *Cajanus cajan* (beans) were planted per pot. The plants were grown in a controlled screen-house environment to minimize external variability.

GROWTH CONDITIONS

Consistent watering and light conditions were maintained for all pots. Temperature and humidity were monitored and recorded throughout the experiment.

SAMPLING AND DATA COLLECTION

The plants were allowed to grow for five weeks after planting (WAP). At the end of the growth period, growth parameters such as plant height and stem girth were measured.

METHODS

Leaves and stems were harvested from each treatment group, and tissue extracts were prepared for biochemical assays.

DPPH FREE RADICAL SCAVENGING ACTIVITIES

Free radical scavenging was evaluated by determination of the DPPH free radical activity according to the methods of Tang, *et al.,* (2001). 1ml 0.3mM of 1,1-diphenyl-2-pirerylhydrazyl (DPPH) in 100% ethanol was added to a test-tube of containing 4ml of the extract . A control was prepared by adding 1 ml of DPPH solution to 4ml of 70% ethanol. Following storage in the dark for 30 minute, the absorbance was read at 517nm using a U/V visible spectrophotometer. The percentage of the free radical activity was calculated based on the following equation.

Free radical scavenging activity (%)= $\{1-\frac{Aborsbance\ of\ sample\ at\ 517nm}{Absorbance\ of\ control}\}$

FRAP (FERRIC REDUCING ANTIOXIDANT POWER) ASSAY

The FRAP reagent was prepared using a previously described method (Benize and strain 1999). In brief, 300mM acetate buffer (pH3.6). 10 mM TPTZ (2, 4, 6-tripyridyl-s-triazine) solution in 40mM hydrochloric acid, and 20mM iron (II) chloride were mixed in a 10:1:1 ratio. FRAP reagent (150µL) was mixed with 20µL of the sample, 20µL of (blank). The absorbance of each was measured at 543nm. The FRAP value was calculated using the following equation:

FRAP value=$\{(A_1-A_0)/(A_c-A_0)x2$,

Where A_c is the positive control, A_1 is the absorbance of the sample, A_0 is the absorbance of the blank.

STATISTICAL ANALYSIS

Analyze data using ANOVA to compare means across treatment groups. Determine

significance at $p<0.05$ and use post-hoc tests for pairwise comparisons.

RESULTS

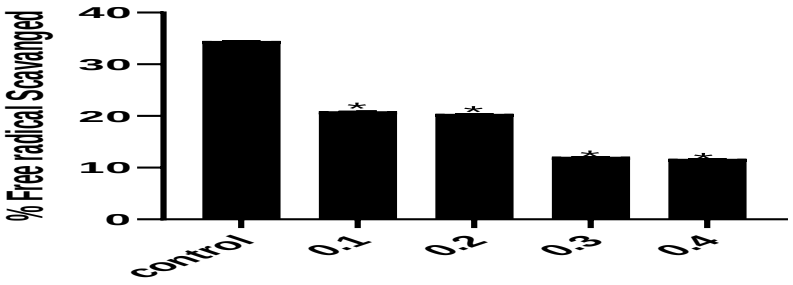

Figure 1. Effect of oil contaminated soil on the DPPH Radical Scavenging ability of pigeon pea. Data are presented as mean ± SEM for three independent experiment done in triplicates *Significant lower than the control

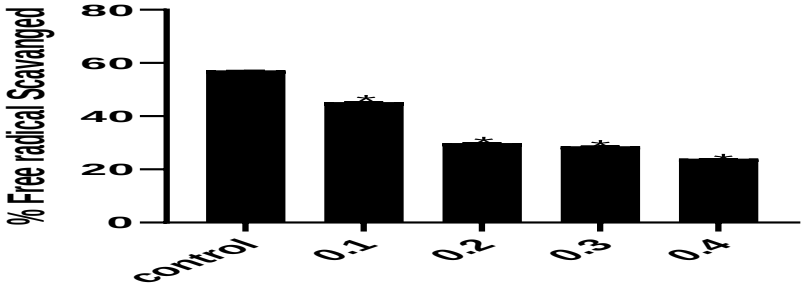

Figure 2. Effect of oil contaminated soil on the DPPH Radical Scavenging ability of maize. Data are presented as mean ± SEM for three independent experiment done in triplicates *Significant lower than the control

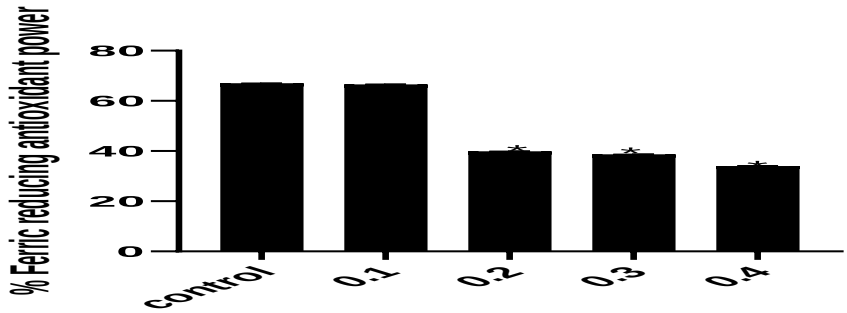

Figure 3. Effect of oil contaminated soil on the Ferric reducing antioxidant power of maize. Data are presented as mean ± SEM for three independent experiment done in triplicates *Significant lower than the control

DISCUSSION

The findings of this study demonstrate that oil-contaminated soil significantly impairs the antioxidant systems of *Cajanus cajan* and *Zea mays*. The reduction in DPPH radical scavenging activity suggests a diminished ability to neutralize free radicals, while the decreased FRAP values indicate reduced electron-donating capacity.

These effects can be attributed to the presence of toxic hydrocarbons and associated compounds in contaminated soil, which interfere with plant metabolic processes. Oil pollution has been reported to inhibit the biosynthesis of phenolic and flavonoid compounds, key contributors to antioxidant activity (Akinola *et al.*, 2021; Ekpo and Nwaankpa, 2022).

Additionally, contaminated soil conditions may impair nutrient uptake and alter enzymatic activities, further reducing antioxidant production. Plants under stress often redirect energy toward survival rather than secondary metabolite synthesis, leading to decreased accumulation of bioactive compounds (Uzoekwe and Oghosanine, 2021).

The consistency of reduced antioxidant activity across both plant species suggests a broad negative impact of oil contamination on plant biochemical functions. This has significant implications for food quality, as reduced antioxidant levels may lower the nutritional and health benefits of these crops.

CONCLUSION

Oil contamination of soil significantly reduces the antioxidant capacity of pigeon pea and maize, as evidenced by decreased DPPH radical scavenging activity and ferric reducing antioxidant power. These findings highlight the detrimental effects of petroleum pollution on plant biochemical composition and nutritional quality.

The study emphasizes the need for effective environmental remediation strategies and stricter regulatory measures to protect agricultural systems in oil-affected regions.

CONFLICT OF INTEREST

The authors declare no conflict of interest.

REFERENCES

Adewale, A. B., Folarin, B. R., and Ojo, J. A. (2021). Effects of crude oil pollution on growth and yield parameters of maize (*Zea mays L.*). *African Journal of Agricultural Research*, 16(3), 182–189.

Akinola, R. A., Adewale, O. B., and Olawale, O. O. (2021). Effects of crude oil contamination on antioxidant enzymes in plants. *Environmental Monitoring and Assessment*, *193*(4), 1–10.

Benzie, I. F. F., and Strain, J. J. (1996). The ferric reducing ability of plasma (FRAP) as a measure of antioxidant power. *Analytical Biochemistry*, *239*(1), 70–76.

Ekpo, I. A., and Nwaankpa, I. L. (2022). Phytochemical and antioxidant responses of plants under environmental stress conditions. *Journal of Plant Biochemistry and Biotechnology*, *31*(2), 245–256.

Jahromi, H.K., Farzin, A., Hasanzadeh, E., Barough, S.E., Mahmoodi, N., Najafabadi, M.R.H., Farahani, M.S.,

Mansoori, K., Shirian, S., and Ai, J. (2020). Enhanced Sciatic Nerve Regeneration by Poly-L-Lactic Acid/Multi-Wall Carbon Nanotube Neural Guidance Conduit Containing Schwann Cells and Curcumin Encapsulated Chitosan Nanoparticles in Rat. *Mater. Sci. Eng*. C, 109, 110564.

Okon, I. E., Bassey, R. B., and Etukudo, M. A. (2022). Antioxidant enzyme responses of maize grown in crude oil-polluted soils. *Scientific African*, 15, e01045.

Okonokhua, B. O., Ikhajiagbe, B., Anoliefo, G. O., and Emede, T. O. (2020). The effects of spent engine oil on soil properties and growth of maize (*Zea mays* L.). *Journal of Applied Sciences and Environmental Management, 24*(3), 475–482.

Saikol, S., Kumar, B.; Shishodia, G., Koul, S., and Koul, H.K. (2019). Reactive Oxygen Species and Cancer: A Complex Interaction. *Cancer Lett.* , 452, 132–143.

Tang, X., He, Z., Dai, Y., Xiong , Y.l., Xie, M., and Chen, J. (2001). Peptide fractionation and free radical scavenging activity of zein hydrolsate. *Journal of Agricultural and Food chemistry*, 49(2), 131-136.

Uzoekwe, S. A., and Oghosanine, F. A. (2021). The effect of crude oil contamination on soil properties and plant growth. *International Journal of Environmental Science and Technology, 18*(5), 1305–1316.